

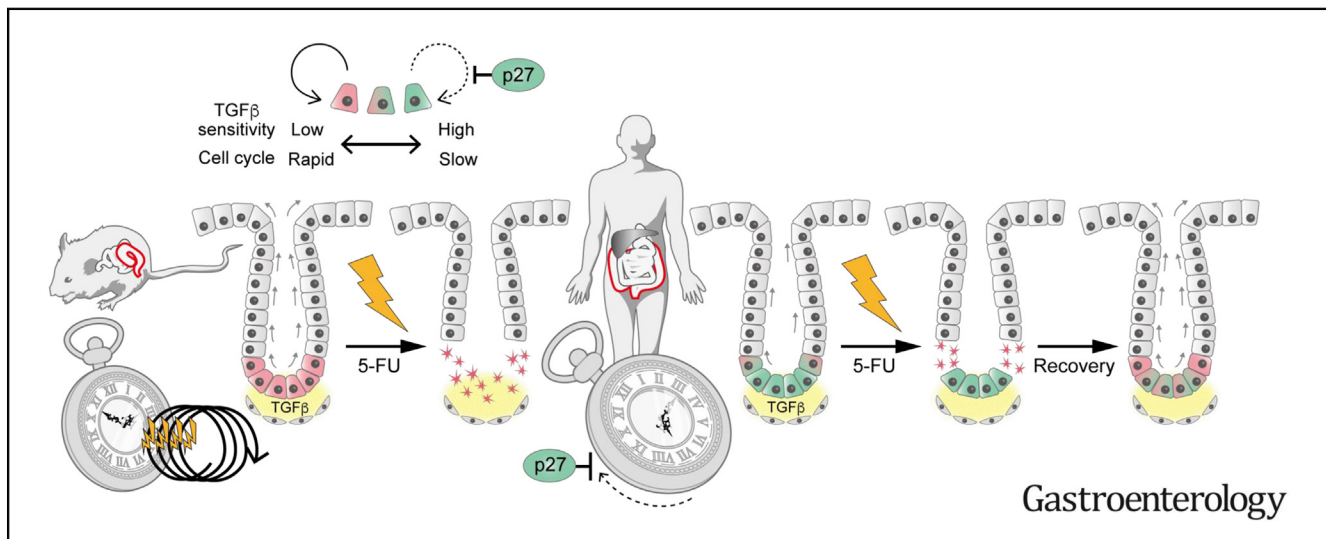
COLON

Identification of Quiescent LGR5⁺ Stem Cells in the Human Colon



Keiko Ishikawa,^{1,2} Shinya Sugimoto,^{1,2} Mayumi Oda,¹ Masayuki Fujii,¹ Sirirat Takahashi,¹ Yuki Ohta,¹ Ai Takano,¹ Kazuhiro Ishimaru,¹ Mami Matano,¹ Kosuke Yoshida,^{1,2} Hikaru Hanyu,¹ Kohta Toshimitsu,¹ Kazuaki Sawada,³ Mariko Shimokawa,¹ Megumu Saito,^{1,4} Kenta Kawasaki,^{1,2} Ryota Ishii,⁵ Koji Taniguchi,^{6,7} Takeshi Imamura,⁸ Takanori Kanai,² and Toshiro Sato¹

¹Department of Organoid Medicine, Sakaguchi Laboratory, Keio University School of Medicine, Tokyo, Japan; ²Department of Gastroenterology, Keio University School of Medicine, Tokyo, Japan; ³Center for Integrated Medical Research, School of Medicine, Keio University, Tokyo, Japan; ⁴Fujii Memorial Research Institute, Otsuka Pharmaceutical Company, Limited, Shiga, Japan; ⁵Department of Biostatistics, Faculty of Medicine, University of Tsukuba, Ibaraki, Japan; ⁶Department of Microbiology and Immunology, Keio University School of Medicine, Tokyo, Japan; ⁷Department of Pathology, Faculty of Medicine and Graduate School of Medicine, Hokkaido University, Sapporo, Japan; and ⁸Department of Molecular Medicine for Pathogenesis, Ehime University Graduate School of Medicine, Ehime, Japan



BACKGROUND & AIM: In the mouse intestinal epithelium, Lgr5⁺ stem cells are vulnerable to injury, owing to their predominantly cycling nature, and their progenies de-differentiate to replenish the stem cell pool. However, how human colonic stem cells behave in homeostasis and during regeneration remains unknown. **METHODS:** Transcriptional heterogeneity among colonic epithelial cells was analyzed by means of single-cell RNA sequencing analysis of human and mouse colonic epithelial cells. To trace the fate of human colonic stem or differentiated cells, we generated LGR5-tdTomato, LGR5-iCasase9-tdTomato, LGR5-split-Cre, and KRT20-ERCreER knock-in human colon organoids via genome engineering. p27⁺ dormant cells were further visualized with the p27-mVenus reporter. To analyze the dynamics of human colonic stem cells in vivo, we orthotopically xenotransplanted fluorescence-labeled human colon organoids into immune-deficient mice. The cell cycle dynamics in xenograft cells were evaluated using 5-ethynyl-2'-deoxyuridine pulse-chase

analysis. The clonogenic capacity of slow-cycling human stem cells or differentiated cells was analyzed in the context of homeostasis, LGR5 ablation, and 5-fluorouracil-induced mucosal injury. **RESULTS:** Single-cell RNA sequencing analysis illuminated the presence of nondividing LGR5⁺ stem cells in the human colon. Visualization and lineage tracing of slow-cycling LGR5⁺p27⁺ cells and orthotopic xenotransplantation validated their homeostatic lineage-forming capability in vivo, which was augmented by 5-FU-induced mucosal damage. Transforming growth factor- β signaling regulated the quiescent state of LGR5⁺ cells. Despite the plasticity of differentiated KRT20⁺ cells, they did not display clonal growth after 5-FU-induced injury, suggesting that occupation of the niche environment by LGR5⁺p27⁺ cells prevented neighboring differentiated cells from de-differentiating. **CONCLUSIONS:** Our results highlight the quiescent nature of human LGR5⁺ colonic stem cells and their contribution to post-injury regeneration.

Keywords: Organoids; Slow-Cycling Stem Cell; Intestinal Stem Cell; TGF- β Signaling.

Tissue stem cells are defined as cells with long-term self-renewal and multidifferentiation capacities.¹ Cellular quiescence or dormancy, albeit not included in this definition, has long been considered as another hallmark of tissue stem cells.² Quiescence is a reversible nondividing G₀ state, characterized by minimal energy consumption, low RNA content, and reduced protein synthesis. These characteristics are known to prevent hematopoietic and muscle stem cells from premature exhaustion.³ The quiescent cells were identified in the mouse intestinal epithelium at the fourth cellular position from the crypt base using label-retaining assay, hence referred to as "label-retaining cells" (LRCs) or +4 cells.⁴ However, whether LRCs have stemness has been controversial for decades. Recent development of genetic lineage tracing systems has reconciled this issue by demonstrating that cycling Lgr5⁺ cells, rather than LRCs, behave as intestinal stem cells (ISCs) in homeostasis.⁵ LRCs commit to differentiation, yet can revert to ISCs only after depletion of pre-existing ISCs by injury.⁶⁻¹² Although mouse genetic models have provided clear-cut evidence for the cell cycle state of ISCs, whether this framework applies to human ISCs has been obscure due to the lack of experimental systems.

Organoid technology has emerged as a key experimental tool to assess the functionality of human ISCs.¹³ We recently established an orthotopic xenotransplantation technique that engrafts human colon organoids onto the surface of epithelium-removed mouse colon. A combination of orthotopic xenotransplantation and genetic lineage tracing validated the existence and functionality of human colonic stem cells (hCoSCs) in a tissue context.¹⁴ Contrary to Lgr5⁺ cells in the surrounding mouse tissue, most human LGR5⁺ cells were Ki67-negative, suggesting that hCoSCs are slowly cycling. The expression of Ki67, however, provides only snapshot information on cell cycle states, and it remains unclear whether the low Ki67 positivity among hCoSCs reflects the G₁ transition of cycling cells or cell-intrinsic quiescence. To address these questions, we obtained a panorama of human colonic epithelial cells using single-cell RNA sequencing (scRNA-seq) and identified a nondividing subpopulation in human LGR5⁺ colonic cells. By leveraging genetic lineage tracing and orthotopic xenotransplantation, we demonstrated the stemness of slow-cycling human LGR5⁺ cells in homeostasis and during regeneration. Our findings not only highlight the difference in ISC biology between mice and humans, but they also lay a foundation for future research that aspires to control or facilitate regenerative response in the human gut.

Methods

Human Tissues

A healthy human colon sample for scRNA-seq was obtained from the resected specimen of a 78-year-old woman with ascending colon cancer. The tissue was sampled from the

WHAT YOU NEED TO KNOW

BACKGROUND AND CONTEXT

Mouse Lgr5⁺ stem cells are cycling rapidly and injury-sensitive. However, the dynamic behavior of human colonic stem cells in homeostasis and during regeneration remains unclear.

NEW FINDINGS

Combination of organoids, genome editing, and transplantation technologies demonstrated that human LGR5^{+p27⁺ cells are slow-cycling colon stem cells. LGR5^{+p27⁺ cells are resistant to injury and fuel mucosal regeneration after chemotherapy.}}

LIMITATIONS

Given our small cohort size, whether the cell cycle duration of LGR5^{+p27⁺ cells is affected by the individual's background, such as sex, age, and ethnicity, remains uncertain.}

IMPACT

By harmonizing organoid technology with genome editing and orthotopic transplantation, we were able to investigate the functional dynamics of human colonic stem cells in a near-native tissue context.

normal mucosa 10 cm from the tumor. Normal colonic organoids were established previously from the ascending colon of a 68-year-old woman and from the descending colon of a 68-year-old man.¹⁴ All procedures were approved by the ethics committees at Keio University Hospital and Tokyo University Hospital.

Mice

All animal procedures were approved by the Keio University School of Medicine Animal Care Committee. Male NOD/Shi-scid, IL-2R γ^{null} mice (5–6 weeks old) and C57BL/6 mice were obtained from the Central Institute for Experimental Animals (Kawasaki, Japan). Orthotopic xenotransplantation of human colonic organoids was performed as described previously.¹⁴ We obtained mouse colonic crypts from 3 female 12-week-old C57BL/6 mice for scRNA-seq using the same procedures for human crypt isolation.

Culture and Gene Engineering of Organoids

We cultured human colonic organoids as described previously.¹⁵ We generated LGR5-iCasase9-tdTomato (LGR5-iCT), LGR5-CreER, LGR5-split-Cre, and KRT20-ERCreER knock-in organoids. The split-Cre system was designed as reported previously.⁸ For visualization of p27, the p27-mVenus reporter

Abbreviations used in this paper: CreC, C-terminal domain of Cre; CreN, N-terminal domain of Cre; EdU, 5-ethynyl-2'-deoxyuridine; 5-FU, 5-fluorouracil; hCoSC, human colonic stem cell; ISC, intestinal stem cell; LGR5-iCT, LGR5-iCasase9-tdTomato; LRC, label-retaining cell; scRNA-seq, single-cell RNA sequencing; TGF- β , transforming growth factor- β .

Most current article

© 2022 The Author(s). Published by Elsevier Inc. on behalf of the AGA Institute. This is an open access article under the CC BY-NC-ND license (<http://creativecommons.org/licenses/by-nc-nd/4.0/>).

0016-5085

<https://doi.org/10.1053/j.gastro.2022.07.081>

(a gift from T. Kitamura, Tokyo University)¹⁶ was introduced into the human colonic organoids. Mouse colonic organoids were established from 12-week-old Lgr5-DTR-EGFP male mice (a gift from F. J. de Sauvage). Additional details are described in the *Supplementary Methods*.

Results

Single-Cell Characterization of Human Colonic Stem Cells

To survey the transcriptomes of human colonic epithelial cells, we conducted an scRNA-seq analysis of the human colonic epithelium. Unsupervised clustering partitioned human colonic epithelial cells into 10 subpopulations, of which 5 subpopulations represented differentiated cell subtypes based on the gene expression profile, including colonocyte-1, colonocyte-2, goblet cell-1, goblet cell-2, and BEST4/OTOP2 cell^{17,18} (Figure 1A, *Supplementary Figure 1A*). Among the other 5 immature subpopulations was an LGR5⁺ stem cell subpopulation characterized by the distinct expression of stem cell markers *LGR5*, *ASCL2*, and *SMOC2* (Figure 1B, *Supplementary Figure 1A*). A secretory progenitor subpopulation expressed its known markers, including *NEUROG3*, *HES6*, *PROX1*, *SOX4*, and the proliferation marker *STMN1* (Figure 1B, *Supplementary Figure 1A* and B). This subpopulation also exhibited high levels of LRC and Mex3a signatures,^{7,8} reminiscent of +4 cells in the mouse small intestine (Figure 1B, *Supplementary Figure 1B*). The other 3 immature populations were considered to be transit amplifying cells, based on their low expression level of differentiation markers and enrichment of cell cycle markers (Figure 1B). A re-analysis of 2 public scRNA-seq datasets validated our results (*Supplementary Figure 1C*).^{17,18}

The LGR5⁺ stem cell subpopulation displayed low expression levels of proliferation markers *MKI67*, *CCNB1*, and *PCNA* (Figure 1B), which contrasted with the predominantly proliferative mouse Lgr5⁺ stem cells. To compare the cycling status between mouse and human CoSCs, we performed scRNA-seq of the mouse colonic epithelium and also retrieved public scRNA-seq data of the mouse colon.^{19,20} A combined analysis of mouse and human colon scRNA-seq data revealed 9 shared subpopulations (Figure 1C, *Supplementary Figure 2A* and B). As described previously,²¹ *BEST4*⁺ cells were absent from the mouse colon. Expression of ISC marker genes distinguished CoSCs in the combined analysis (Figure 1C). The expression of cell cycle genes revealed that most hCoSCs were nondividing, whereas the mouse CoSCs comprised cells in S and G2/M phases (Figure 1D).

To validate the scRNA-seq results, we analyzed sections of colon tissues. *LGR5* mRNA in situ hybridization and Ki67 immunohistochemistry confirmed the rarity of human Ki67-expressing LGR5⁺ cells (Figure 1E). Ki67 staining of the Lgr5^{GFP} mouse colon validated the proliferative property of mouse colon Lgr5⁺ cells (Figure 1F). Human Ki67⁻LGR5⁺ cells were localized mainly at the crypt bottom, with an inverse topological arrangement compared with mouse

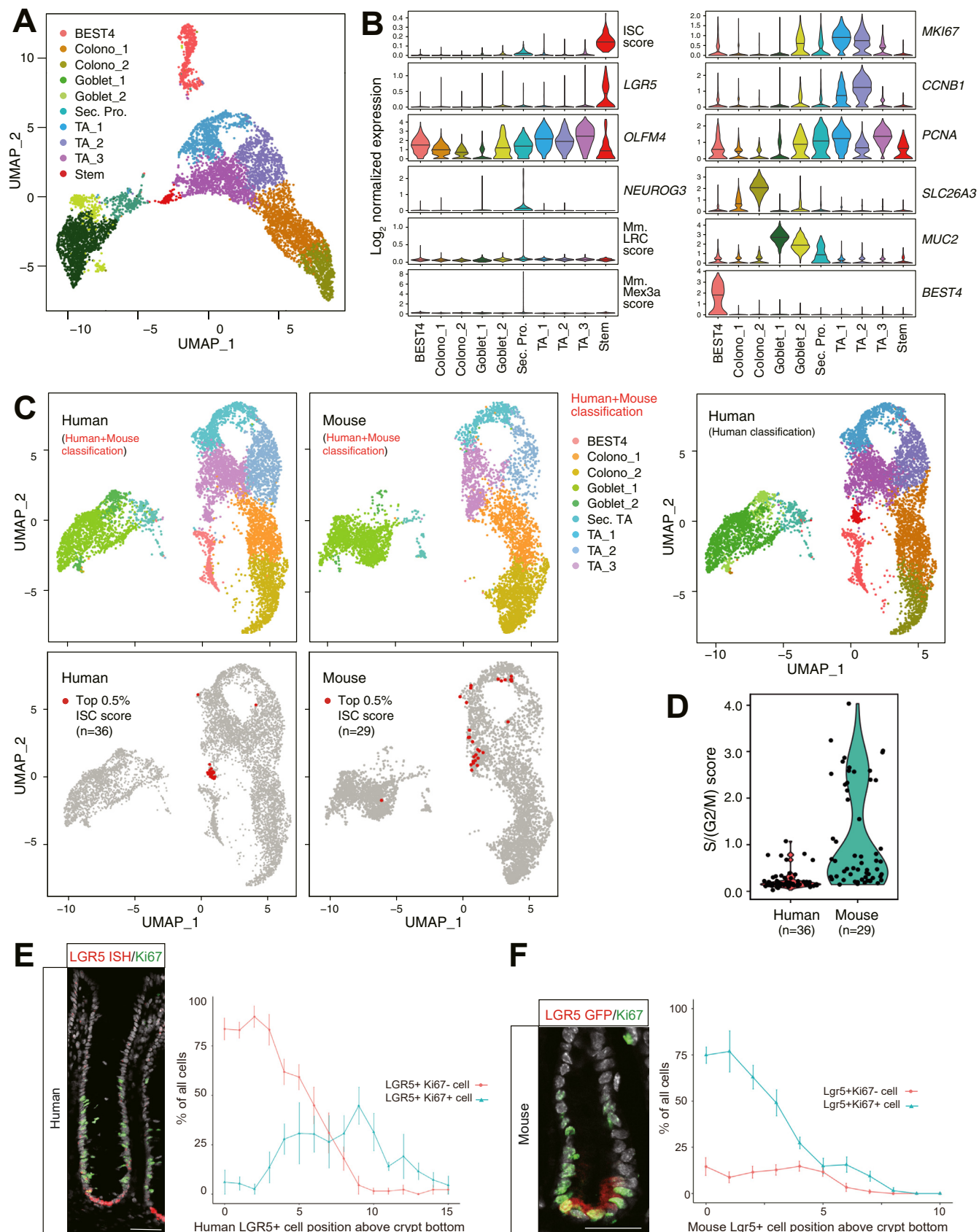
Ki67⁻Lgr5⁺ cells (Figure 1E and F). These results collectively highlighted the unique cycling status and localization pattern of LGR5⁺ hCoSCs.

Identification of Human LGR5⁺p27⁺ Slow-Cycling Stem Cells

Although scRNA-seq illuminated the presence of nondividing LGR5⁺ cells in the human colon, their isolation and functional assessment require identification of their positive markers. With this aim, we referred to the gene expression profile of human colonic organoids and nominated cyclin-dependent kinase inhibitors, p21, p27, and p57, as potential markers for nondividing cells. These cyclin-dependent kinase inhibitors were selectively expressed in Ki67-negative cells, but the specificity for LGR5⁺ cells differed among the markers. p21 and p57 were scarcely expressed in the lower crypt, whereas p27 marked virtually all Ki67⁻ cells at the crypt bottom. As *LGR5* in situ hybridization and p27 immunostaining were technically incompatible, we confirmed the overlap of p27 and *LGR5* expressions using serial section analysis (Figure 2A). p27 was also expressed in upper-crypt Ki67⁻ cells, suggesting p27 as a pan-nondividing cell marker in the human colonic epithelium. Although p27 was also expressed in a minority of Ki67⁻ cells in mouse colonic crypts (*Supplementary Figure 3A*), only a mean \pm SEM of 0.71 ± 0.16 Lgr5⁺p27⁺ cells were found per crypt, in agreement with the cycling status of mouse Lgr5⁺ CoSCs.^{5,22}

We next sought to fluorescently label p27⁺ cells for further characterization of human colon LGR5⁺p27⁺ cells. As the expression level of p27 is regulated by means of ubiquitin-mediated protein degradation, we employed a p27 reporter, in which mVenus is fused to mutant-p27 with no cyclin-dependent kinase inhibitory activity¹⁶ (Figure 2B). The p27-mVenus fusion protein is degraded in parallel with endogenous p27 by the proteasome machinery,²³ and its emission thereby mirrors the endogenous p27 expression. For simultaneous visualization of p27 and LGR5, we introduced p27-mVenus and LGR5-tdTomato reporters into human colonic organoids (Figure 2B). Mutually exclusive expression of p27-mVenus and Ki67 was confirmed in reporter organoids (Figure 2C). Overexpression of p27-mVenus minimally affected the proportion of Ki67⁺ cells in LGR5⁺ cells and organoid growth, excluding its growth-inhibitory effect on human colonic organoids (*Supplementary Figure 3B-E*).

To determine the self-renewal potential of LGR5⁺p27⁺ cells, we next performed a colony-formation assay. Sorted LGR5⁺p27⁺ cells efficiently formed organoids, albeit with reduced competence compared with LGR5⁺p27⁻ cells (Figure 2D-F). A similar result was obtained from another LGR5-tdTomato/p27-mVenus reporter line derived from an independent donor (Figure 2E and F). Double staining of Pyronin Y and Hoechst 33342 revealed that 83% and 43% of sorted LGR5⁺p27⁺ and LGR5⁺p27⁻ cells were in the G₀ phase, respectively, indicating efficient detection of the nonproliferative status by the p27 reporter (Figure 2G). To further delineate the dynamics of LGR5⁺p27⁺ cells, we



performed single-cell resolution live imaging of reporter colon organoids. LGR5⁺p27⁺ cells rarely divided and maintained stable p27 and LGR5 expression during a 64-hour observation (Figure 2H). Approximately 10% of LGR5⁺p27⁺ cells became LGR5⁺p27⁻ cells and proliferated subsequently, indicating the reversibility of the G₀ state in LGR5⁺p27⁺ cells. In contrast to LGR5⁺p27⁺ cells, LGR5⁺p27⁻ cells were expanding rapidly. Approximately one-half of the LGR5⁺p27⁻ cells eventually produced at least 1 LGR5⁺p27⁺ cell, whereas the remaining one-half lost LGR5 expression, presumably due to differentiation. These results suggested that LGR5⁺p27⁻ cells are more prone to differentiation than LGR5⁺p27⁺ cells in *in vitro* organoid culture (Supplementary Figure 3F).

Lack of Lgr5⁺p27⁺ Slow-Cycling Stem Cells in the Mouse Colon Epithelium

To compare the cell cycle behavior of CoSCs between humans and mice, we introduced the p27-mVenus reporter into Lgr5-GFP mouse colon organoids. Consistent with the expression pattern in the native tissue (Supplementary Figure 3A), Ki67⁻ cells in mouse colon organoids sporadically displayed dim p27-mVenus reporter expression (Supplementary Figure 3G and H). Live imaging revealed that more than one-half of Lgr5⁺p27⁺ cells lost p27-mVenus expression within 1 day (Supplementary Figure 3I). Given the evanescent p27 reporter expression during early G₁/late G₁ transition in a previous report,¹⁶ the p27 expression in mouse Lgr5⁺ cells is likely to reflect their early G₁ state rather than G₀ status. Together, human and mouse colon LGR5⁺ cells showed distinct cell cycle behaviors in an identical culture environment.

Human Colon LGR5⁺p27⁺ Cells Behave as Label-Retaining Cells in a Tissue Context

To investigate the dynamics of LGR5⁺ hCoSCs *in vivo*, we generated orthotopic intraluminal xenografts of human colon organoids, as described previously.¹⁴ Briefly, we detached the native epithelium from the distal colon of immune-deficient mice using EDTA, and replaced the epithelium with human colonic organoids by infusing the organoids through the anus. After stable implantation, we performed whole-exome sequencing and RNA-seq analyses of the original organoids, LGR5-tdTomato/p27-mVenus reporter organoids and xenograft-derived organoids to

exclude possible accrual and enrichment of specific genomic abnormalities during gene engineering and xenotransplantation procedures. These analyses indicated the similarity of transcriptome profiles and the lack of conspicuous copy-number alterations among the samples (Supplementary Figure 4A and B).

After being xenotransplanted onto the epithelium-denuded mouse colon, LGR5⁺p27⁺ cells were positioned at the crypt bottom, mirroring their localization in the human colon (Figure 3A). To determine the cycling behavior of LGR5⁺p27⁺ cells, we administered 5-ethynyl-2'-deoxyuridine (EdU) to xenograft-bearing mice. Upon a 1-hour treatment, EdU marked the cells in the proliferating zone, while sparing the crypt bottom (Supplementary Figure 5A and B). This incorporation pattern was compatible with previous *in vivo* human studies using ³H-thymidine administration.^{24,25} A continuous 1-day and 4-day EdU treatment labeled virtually all LGR5⁺ cells above the +4 position and approximately 17% and 60% of LGR5⁺ cells at the crypt bottom, respectively. Based on these EdU incorporation rates, the duration of cell cycle in LGR5⁺ cells residing above the +4 position or at the crypt bottom was estimated to be 1.5 days or 7.3 days, respectively. After a 14-day or 21-day EdU washout (Supplementary Figure 5A and C), LRCs were observed in a mean ± SEM of 20.1% ± 2.6% (14 days) or 5.6% ± 0.7% (21 days) of LGR5⁺ cells in xenografts, but were absent from the surrounding mouse colon epithelium (Supplementary Figure 5C-E), consistent with previous reports.^{26,27} However, more than one-half of LRCs expressed LGR5 (Supplementary Figure 5F). The remaining LGR5-negative LRCs were mostly enteroendocrine cells (Supplementary Figure 5G). We then orthotopically xenotransplanted LGR5-tdTomato/p27-mVenus organoids and confirmed that most of the LGR5⁺LRCs co-expressed the p27 reporter (Figure 3B and C). These results indicate the existence of LRCs in the human colon, as well as the fidelity of the p27-mVenus reporter in the xenograft model.

Transforming Growth Factor-β Signaling Regulates the Dormancy of Human Colonic Stem Cells

We next sought to determine the mechanism that regulates the p27⁺ state in hCoSCs. During the culture of organoids, we fortuitously found that removal of a transforming growth factor-β (TGF-β) inhibitor markedly increases the

Figure 1. Nondividing LGR5⁺ stem cells in the human colonic epithelium. (A) A uniform manifold approximation and projection (UMAP) plot of single cell transcriptomes derived from 7103 human colonic epithelium cells. Transit amplifying (TA) cells are classified into 3 clusters based on cycling status. Colono, colonocyte; Sec. Pro., secretory progenitor cell. (B) The expression of ISC-related genes (ISC score, LGR5, and OLFM4), secretory precursor gene (NEUROG3), mouse LRC, and Mex3a signature scores. The expression of cell cycle genes and differentiation-related genes in each cluster. The levels of ISC, LRC, and Mex3a signature scores refer to the abundance of signature gene transcripts in percents. The expressions of single genes are shown in log₂-transformed normalized counts. (C) Integrated scRNA-seq analysis of the mouse and human colonic epithelium. Cells with a top 0.5% ISC score are highlighted in red. A UMAP plot of human colonic epithelium cells using human-specific classification used in Figure 1A is shown. (D) Distribution of the S and G2/M phase scores in human and mouse colonic stem cells. (E) Co-staining of Ki67 with LGR5 *in situ* hybridization (ISH) in a human colon. Scale bar: 50 μm. Mean cell position of LGR5⁺Ki67⁺ and LGR5⁺Ki67⁻ cells in human colonic crypts. (F) Ki67 staining and the expression of Lgr5-GFP reporter in a mouse colon. Scale bar: 25 μm. Mean cell position of Lgr5⁺Ki67⁺ and Lgr5⁺Ki67⁻ cells in mouse colonic crypts.

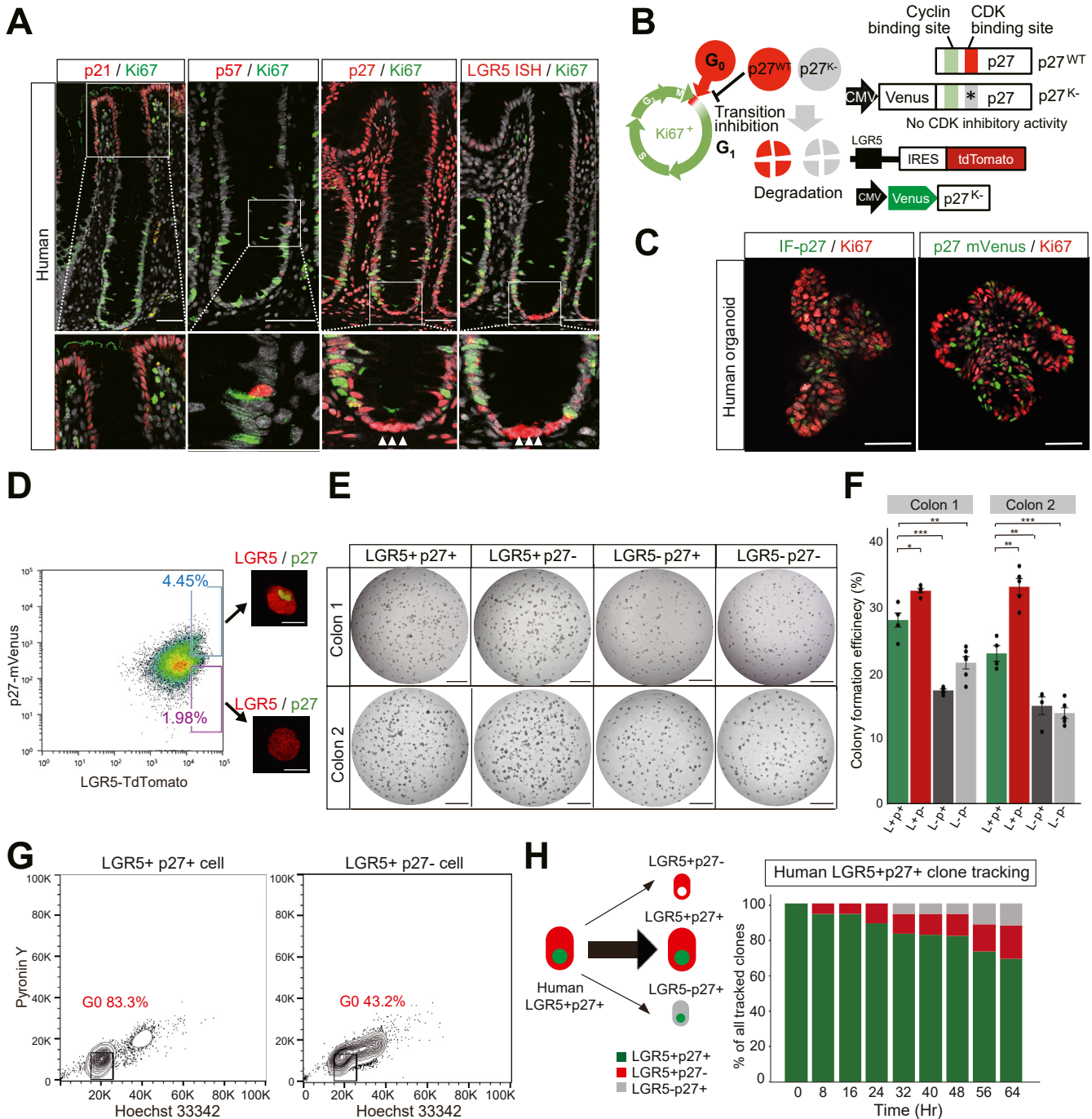
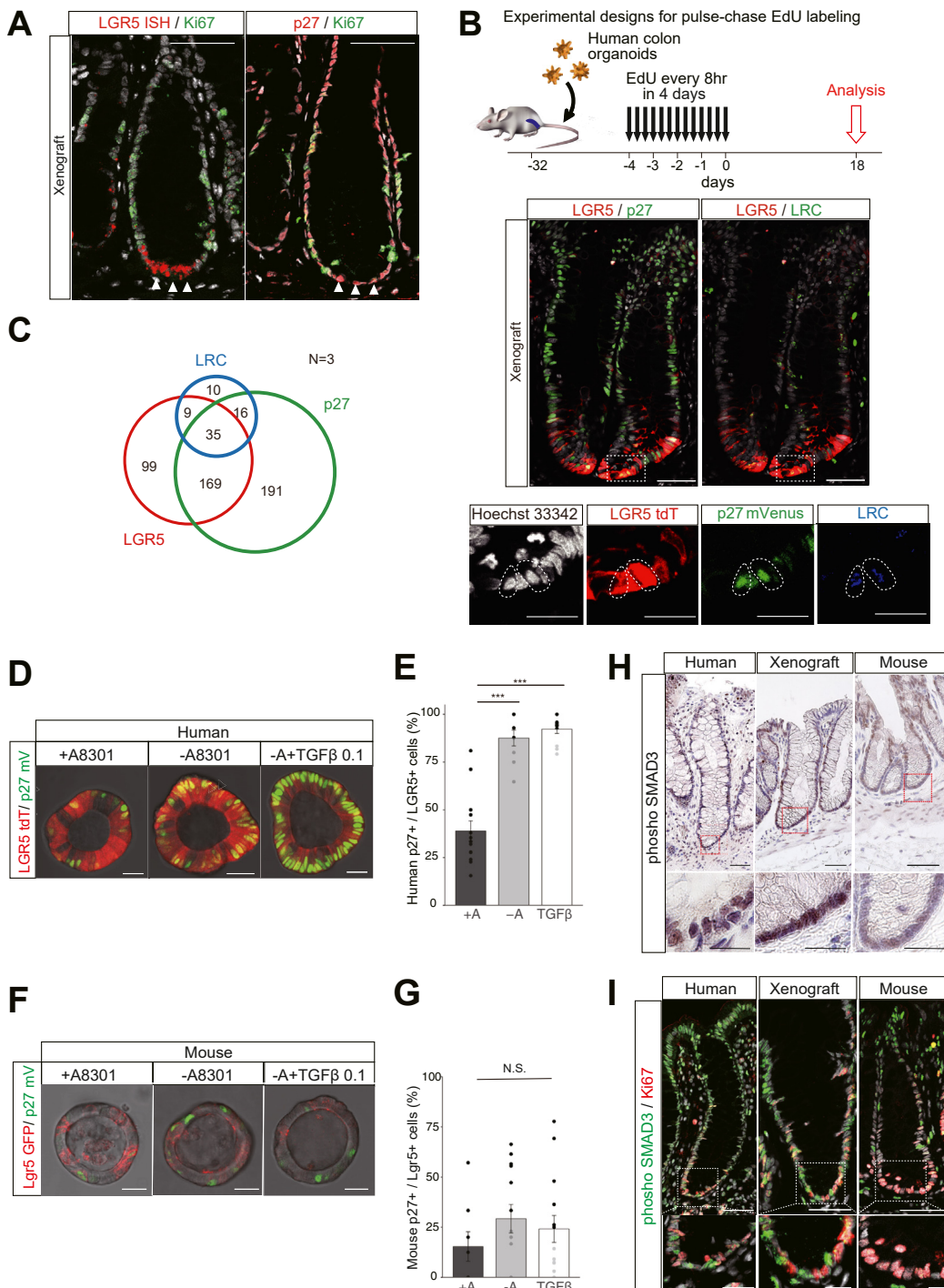


Figure 2. Fluorescence labeling of nondividing LGR5⁺ hCoSCs. (A) Co-staining of Ki67 with p21, p57, or p27 in a human colon tissue. p21 and p57 are not expressed at the crypt bottom. Co-staining of Ki67 with LGR5 in situ hybridization and p27 using serial sections of a human colon. Arrowhead shows LGR5⁺Ki67⁻ cells at the crypt base in the human sample. Note the expression of p27 in LGR5⁺Ki67⁻ cells. Scale bar: 50 μ m. (B) The workings of the p27-mVenus reporter. The reporter was introduced to LGR5-TdTomato organoids for the visualization of nondividing CoSCs. (C) Co-staining of p27 and Ki67 staining in a human colon organoid. Ki67 immunofluorescence and p27-mVenus fluorescence in a reporter colon organoid. Scale bar: 50 μ m. (D) Gating strategy for sorting LGR5⁺p27⁺ and LGR5⁺p27⁻ cells in LGR5-TdTomato/p27-mVenus organoids. LGR5⁺p27⁺ cells and LGR5⁺p27⁻ cells were confirmed by confocal imaging as shown by the representative images. Scale bar: 10 μ m. (E) In vitro colony formation from sorted LGR5⁺p27⁺, LGR5⁺p27⁻, LGR5⁻p27⁺, and LGR5⁻p27⁻ cells organoids; 1000 cells were plated. Scale bar: 1 mm. (F) Colony-formation efficiency of sorted LGR5⁺p27⁺ cells, LGR5⁺p27⁻ cells, LGR5⁻p27⁺ cells, and LGR5⁻p27⁻ cells. Data are shown as mean \pm SEM. A dot represents each well. Analysis of variance 5, 5, 5, and 6 wells for LGR5⁺p27⁺, LGR5⁺p27⁻, LGR5⁻p27⁺ and LGR5⁻p27⁻ cells (colon 1), and 4, 5, 4, and 5 wells for LGR5⁺p27⁺, LGR5⁺p27⁻, LGR5⁻p27⁺, and LGR5⁻p27⁻ cells (colon 2). (G) Cell-cycle analysis of sorted LGR5⁺p27⁺ and LGR5⁺p27⁻ cells. Cells in the G₀ phase are gated on the basis of low DNA (Hoechst 33342) and RNA (pyronin Y) contents. (H) The cell fate of human LGR5⁺p27⁺-derived clones. No LGR5⁺p27⁺ clones became LGR5⁻p27⁻ cells during the observation period. The percentage of each cell fate in all tracked LGR5⁺p27⁺ clones at multiple time points are shown. n = 35 clones from 14 human organoids.

number of LGR5⁺p27⁺ cells in human colon organoids (Figure 3D and E). As reported previously for colorectal cancer organoids,²⁸ TGF- β 1 treatment at a high concentration (1 ng/mL) strongly induced p27 expression in both human and mouse colon organoids (Supplementary Figure 5H). The high-dose TGF- β 1 treatment also reduced the expression of LGR5-transcript and -reporter in colon

organoids, suggesting differentiation (Supplementary Figure 5H and I). Interestingly, treatment with low-dose TGF- β 1 (0.1 ng/mL) similarly increased p27⁺ cells in human colon organoids, although not affecting the LGR5 level (Figure 3D and E, Supplementary Figure 5I). The induction of p27 by low-dose TGF- β 1 treatment was attenuated in mouse colon organoids, suggesting the difference in TGF- β



sensitivity between the 2 species (Figure 3F and G). Therefore, the quiescent state of hCoSCs may reflect their relatively higher sensitivity to TGF- β .

We next analyzed TGF- β activation status in patient colon tissues using immunohistochemistry. SMAD3 phosphorylation, which indicates active TGF- β signaling, was evident at the colonic epithelium surface (Figure 3H and I). After signal enhancement, we detected phospho-SMAD3 in Ki67 $^+$ cells at the crypt bottom (Figure 3J). The specificity of phospho-SMAD3 staining was validated using TGF- β inhibitor-treated and TGF- β -treated organoids (Supplementary Figure 5J). Consistently, we detected SMAD3 phosphorylation in the crypt bottom cells of orthotopic xenografts, but not in those of the surrounding mouse epithelium (Figure 3H). Re-analysis of a public scRNA-seq dataset of the human colon revealed mRNA expression of *TGF β 1* predominantly in endothelial cells, implying their role as a TGF- β ligand supplier (Supplementary Figure 5K).¹⁸ These results suggest that the quiescent status and p27 expression in human colonic crypt base cells are regulated by means of TGF- β signaling.

To further determine the role of TGF- β signaling in the dormancy maintenance, we performed CRISPR-Cas9-mediated knockout of *TGF β R2*, an essential receptor component of TGF- β signaling. Legitimate *TGF β R2* knockout was confirmed by means of Sanger sequencing and resistance to TGF- β treatment (Supplementary Figure 6A). *TGF β R2* knockout organoids did not show SMAD2/3 phosphorylation after TGF- β treatment, indicating complete inactivation of TGF- β signaling (Supplementary Figure 6B). In contrast to the enrichment of LGR5 $^+$ p27 $^+$ cells in TGF- β -treated control organoids, TGF- β treatment failed to increase the number of LGR5 $^+$ p27 $^+$ cells in *TGF β R2*-knockout organoids (Supplementary Figure 6C-E). We further determined the functional effect of TGF- β signal inhibition using xenograft models. *TGF β R2*-knockout xenografts were devoid of SMAD2/3 phosphorylation (Supplementary Figure 6F), and showed fewer LGR5 $^+$ p27 $^+$ cells and a higher EdU incorporation rate in LGR5 $^+$ cells compared with control organoid xenografts (Supplementary Figure 6G-I). These results collectively demonstrate the role of TGF- β signaling in the

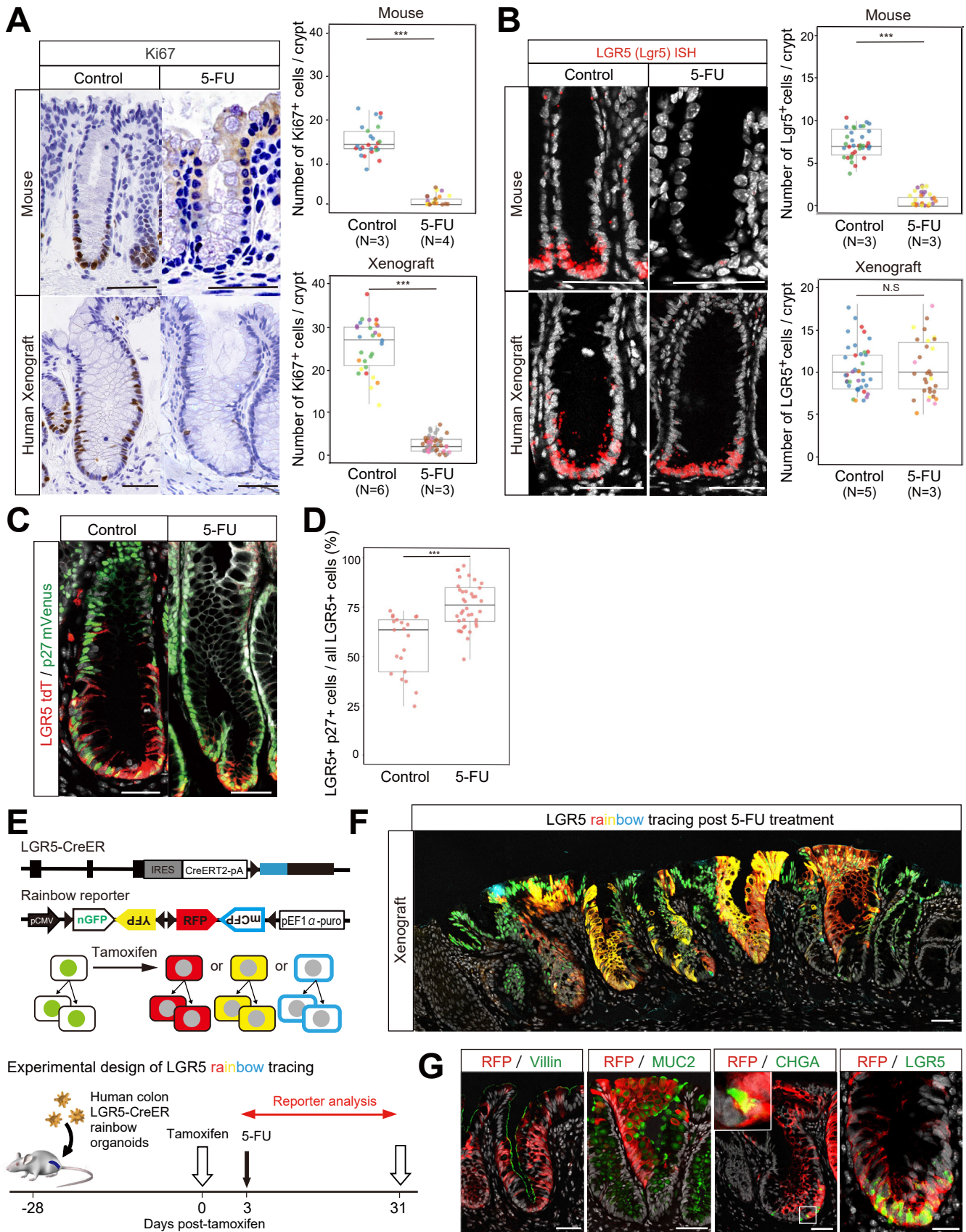
maintenance of slow-cycling LGR5 $^+$ cells in the human colonic epithelium.

LGR5 $^+$ Human Colonic Stem Cells Persist During Chemotherapy

We next explored the functional role of slow-cycling LGR5 $^+$ cells in the human colon epithelium using a chemotherapy-induced injury model. To prospectively analyze whether LGR5 $^+$ p27 $^+$ cells are chemoresistant, we generated LGR5-CreER/LGR5-tdTomato double knock-in human colonic organoids and subsequently introduced the p27-mVenus reporter and the Cre-activatable iRFP-BFP reporter (Supplementary Figure 7A). In vitro live imaging of these organoids allowed us to dynamically capture clonal lineage generation from single LGR5 $^+$ cells, together with information on p27 expression (Supplementary Figure 7B). In a standard culture condition, LGR5 $^+$ p27 $^+$ cells minimally divided and remained p27 $^+$ during the 4-day observation period (Supplementary Figure 7C), whereas LGR5 $^+$ p27 $^-$ cells vigorously propagated yet rarely generated LGR5 $^+$ p27 $^+$ cells (Supplementary Figure 7C). An exposure to 5-FU stalled the proliferation of LGR5 $^+$ p27 $^-$ cells and their lineage formation (Supplementary Figure 7D). Interestingly, LGR5 $^+$ p27 $^+$ cells tolerated 5-FU and underwent cell cycle re-entry, as indicated by the loss of p27 expression (Supplementary Figure 7D). Thus, LGR5 $^+$ p27 $^+$ cells contribute to clonal lineage formation in a steady state, but are mobilized after injury in vitro.

To validate the chemoresistance of LGR5 $^+$ cells in a tissue context, we administered a sublethal dose of 5-FU to mice bearing orthotopic xenografts of LGR5-tdTomato/p27-mVenus organoids. The cytotoxic effect of 5-FU was confirmed by the loss of Ki67 expression in the recipient mouse and donor human epithelia (Figure 4A). Consistent with previous reports,^{6,11,29,30} 5-FU treatment eradicated murine Lgr5 $^+$ CoSCs (Figure 4B). In contrast, LGR5 $^+$ hCoSCs remained in xenografts, indicating CoSCs in mice and humans respond differentially to cytotoxic damage (Figure 4B). In agreement with the eradication of cycling cells, 5-FU treatment enriched p27 $^+$ cells in LGR5 $^+$ cells of

Figure 3. Dynamics and regulation of human LGR5 $^+$ p27 $^+$ CoSCs. (A) Co-staining of Ki67 with *LGR5* in situ hybridization (ISH) and p27 using serial sections of a orthotopic xenograft. Arrowhead shows LGR5 $^+$ Ki67 $^+$ cells at the crypt base. Note their p27 expression. Scale bar: 50 μ m. (B) EdU pulse-chase labeling in LGR5-tdTomato/p27-mVenus orthotopic xenografts. EdU incorporation was analyzed on day 18 after the last EdU treatment. Representative images of LGR5-tdTomato, p27-mVenus, and EdU $^+$ LRCs in a xenograft tissue. Experimental design for pulse-chase EdU labeling (top). LGR5 $^+$ p27 $^+$ LRCs are outlined with white dotted line. Scale bar: 50 μ m (middle) and 20 μ m (bottom). (C) The relationship among LGR5 $^+$ cells, p27 $^+$ cells, and LRCs; 38 crypts from 3 mice were analyzed. The numbers of LGR5 $^+$ cells and p27 $^+$ cells were counted between the crypt bottom and the +10 position. (D) LGR5-tdTomato and p27-mVenus fluorescence in human colonic organoids treated with or without the TGF- β receptor inhibitor A83-01 (500 nM) or with recombinant TGF- β 1 (0.1 ng/mL for 24 hours) in an A83-01-free condition. Scale bar: 25 μ m. (E) The percentage of p27 $^+$ cells in LGR5 $^+$ cells cultured in the indicated conditions. From the left, 13, 9, and 11 organoids were analyzed. ***P < .001 (1-way analysis of variance, followed by Tukey's post-hoc test). (F) Lgr5-GFP and p27-mVenus expression in mouse colonic organoids treated with or without A83-01 (500 nM) or with recombinant TGF- β 1 (0.1 ng/mL) in an A83-01-free condition. Scale bar: 10 μ m. (G) The percentage of p27 $^+$ cells in mouse Lgr5 $^+$ cells cultured in the indicated conditions. From the left, 8, 13, and 14 organoids were analyzed. Not significant (1-way analysis of variance, followed by Tukey's post-hoc test). (H) Phospho-SMAD3 staining in human colon tissues, a human orthotopic xenograft and mouse colon tissues. Scale bar: 50 μ m (top), 20 μ m (bottom). (I) Phospho-SMAD3 and Ki67 immunofluorescence staining in human colon tissues, a human orthotopic xenograft and mouse colon tissues. Scale bar: 50 μ m (top) and 10 μ m (bottom). Data are shown as mean \pm SEM. A dot represents each organoid (E, G).



xenografts (Figure 4C and D). The proportion of Ki67⁺ cells in LGR5⁺ cells increased sharply 10 days after 5-FU treatment, which suggests that LGR5⁺Ki67⁻ cells re-entered the cell cycle (Supplementary Figure 7E-G). Of note, nuclear YAP expression, a hallmark of the regenerative response in the intestine,^{31,32} was not evident in stable xenografts of human colon organoids. 5-FU treatment triggered YAP activation in parallel with the cell-cycle re-entry (Supplementary Figure 7G and H). These results indicate that a common mechanism of YAP activation operates post-injury regeneration of the human colon epithelium.

The presence of human LGR5⁺ cells after chemo-injury suggests the persistence of pre-existing LGR5⁺ cells. However, an alternative scenario is that the original LGR5⁺ cells were lost by means of 5-FU treatment, and LGR5⁺ cells were newly generated from LGR5⁻ cells. To address this possibility, we analyzed clone formation from pre-existing LGR5⁺ cells in 5-FU-treated xenografts. Previously, we described LGR5-CreER/rainbow reporter human colonic organoids that ubiquitously express nuclear GFP and convert their color into either RFP, CFP, or YFP upon tamoxifen treatment.¹⁴ In this system, tamoxifen treatment induced reporter switching, specifically in LGR5⁺ cells of LGR5-CreER/rainbow organoid xenografts (Figure 4E). 5-FU treatment after tamoxifen administration did not abolish clonal lineage formation from LGR5⁺ cells, indicating that pre-existing LGR5⁺ cells maintained self-renewal capacity during chemotherapy (Figure 4F). Clonal ribbon structures also contained differentiated cell types together with crypt bottom LGR5⁺ cells (Figure 4G). These results suggested that LGR5⁺ hCoSCs persisted during 5-FU treatment and subsequently generated multilineage progenies, indicative of their stemness.

LGR5⁺p27⁺ Cells Manifest Stemness in Homeostasis and After Injury in Vivo

Although the above lineage tracing suggests the persistence of LGR5⁺ cells during chemo-injury, the low spatio-temporal resolution left it ambiguous whether the clonal ribbon formation was derived from slow-cycling LGR5⁺ cells or p27⁺LGR5⁺ cells. To more specifically determine the origin of the lineage formation, we sought to trace the

descendants of cells that express both LGR5 and p27 using a split-Cre system⁸ (Figure 5A). We first knocked-in the C-terminal domain of Cre (CreC) into the intact *LGR5* allele of LGR5-tdTomato organoids (Supplementary Figure 8A and B). We then introduced tet-inducible p27-N-terminal domain of Cre (CreN) into LGR5-tdTomato/LGR5-CreC organoids, in which CreN is constantly degraded by proteasome in cycling cells. Each of CreC and CreN was linked with FKBP, such that they fuse together and form the full-form Cre protein by means of dimerizer treatment (Figure 5A). Thus, in this system, functional Cre protein is expressed only when *LGR5* is transcribed and p27 is un-degraded. As a Cre-activatable reporter, we lastly introduced the nGFP-BFP reporter. The resulting organoids ubiquitously expressed nGFP and gave rise to BFP⁺ cells after a treatment with dimerizer/doxycycline (Figure 5A). Ki67 immunostaining confirmed that BFP-traced cells were nondividing (Supplementary Figure 8C). Consistent with the prior result (Supplementary Figure 7D), in vitro live imaging demonstrated that LGR5⁺p27⁺ (BFP-traced) clones persisted during 5-FU treatment and formed ribbons after a 5-FU washout (Supplementary Figure 8D and E). These results indicated the specificity and fidelity of the LGR5-p27 split-Cre system in vitro.

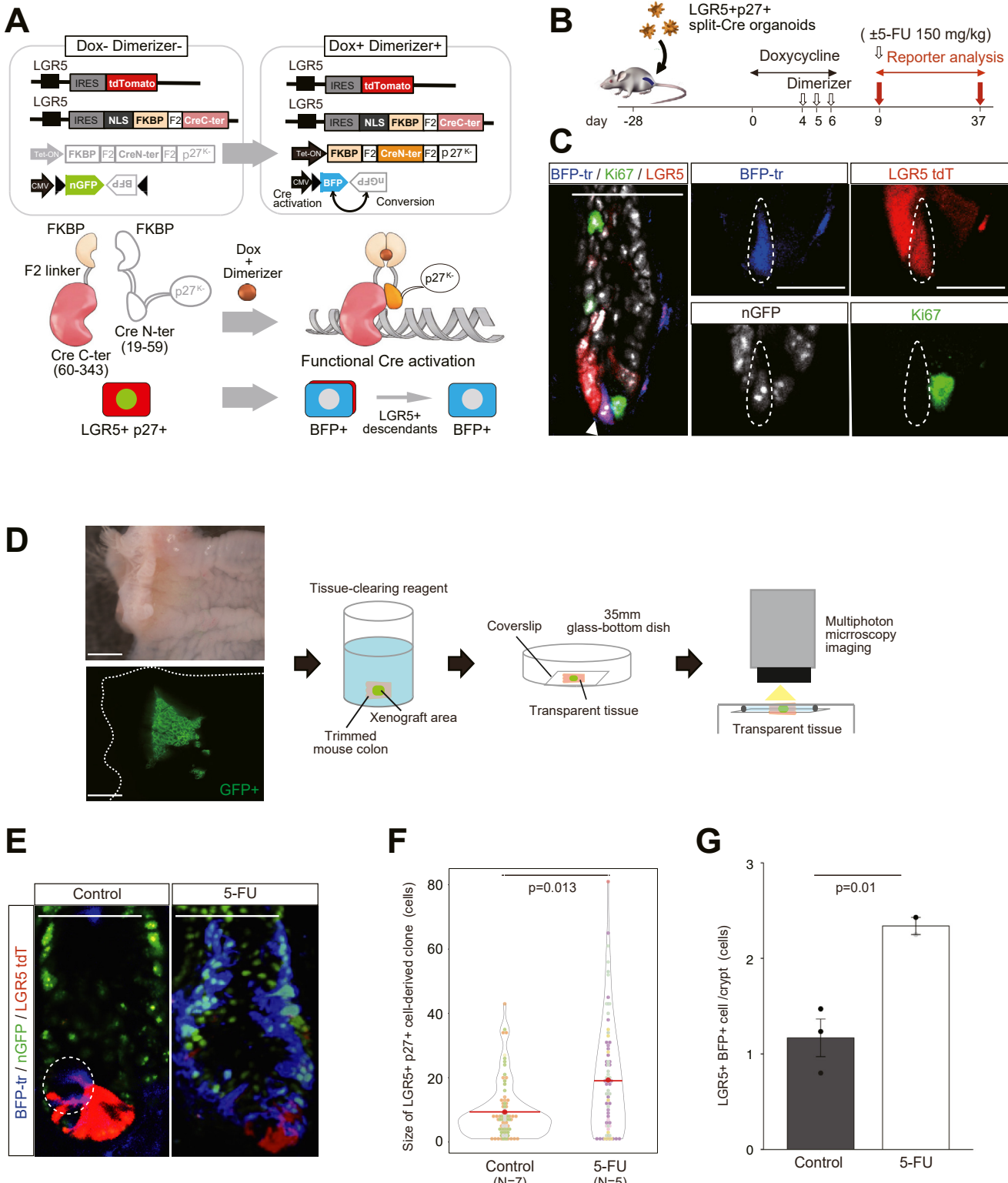
We next investigated the in vivo clonal behavior of LGR5⁺p27⁺ cells using orthotopic xenografts of LGR5-p27 split-Cre organoids (Figure 5B). Most BFP-traced cells were recognized as single cells shortly after administration of dimerizer/doxycycline, and were devoid of Ki67 expression (Figure 5C). One month after tracing, BFP⁺ clones formed small clusters consisting of 3–5 descendants (Figure 5D and E). Even 3 months after the tracing, LGR5⁺p27⁺ cells gave rise to only scattered BFP⁺ clones, whereas a corresponding time frame was sufficient to render mouse colon crypts monoclonal.⁶ Of note, we observed 3 major differentiated cell types (ie, colonocytes, goblet cells, and enteroendocrine cells) in BFP⁺ clones, indicative of the multipotency of LGR5⁺p27⁺ cells (Supplementary Figure 8F). A single short-term EdU labeling 1 month after BFP tracing further depicted generation of cycling LGR5⁺p27⁺EdU⁺ offspring from LGR5⁺p27⁺ cells (Supplementary Figure 8G).

We finally determined whether 5-FU treatment affects the clonal dynamics of LGR5⁺p27⁺ cells. Xenograft-bearing

Figure 4. Human LGR5⁺ CoSCs are resistant to chemo-injury. (A) Ki67 staining in control and 5-FU-treated mouse recipient colon and human colon xenograft tissues. Scale bar: 50 μ m. The percentage of Ki67⁺ cells in each condition. Welch's *t* test. ***P < .001 for mouse Ki67 ($n = 24$ crypts from 3 mice for control, $n = 28$ crypts from 4 mice for the 5-FU-treated group); ***P < .001 for xenograft Ki67 ($n = 30$ crypts from 6 mice for control, $n = 54$ crypts from 3 mice for the 5-FU-treated group). (B) *LGR5* (*Lgr5*) *in situ* hybridization (ISH) in control and 5-FU-treated mouse control colon and human colon xenograft tissues. Scale bar: 50 μ m. The percentage of *LGR5*⁺(*Lgr5*⁺) cells per each crypt. Welch's unpaired *t* test. ***P < .001 for mouse *Lgr5* ($n = 36$ crypts from 3 mice for control, $n = 36$ crypts from 3 mice for the 5-FU-treated group). P > .05 for xenograft *LGR5* ($n = 41$ crypts from 5 mice for control, $n = 31$ crypts from 3 mice for 5-FU-treated group). Not significant. (C) LGR5-tdTomato/p27-mVenus reporter organoid xenografts with or without 5-FU treatment. Scale bar: 50 μ m. (D) The percentage of LGR5⁺p27⁺ cells in all LGR5⁺ cells in control and 5-FU-treated xenografts. Welch's unpaired *t* test. ***P < .001 ($n = 21$ crypts for control, $n = 40$ crypts for 5-FU group). (E) Schedule for the lineage tracing of LGR5⁺ cells in orthotopic xenografts after a single 5-FU treatment. (F) Clonal lineage formation from LGR5⁺ cells in xenograft tissues after 5-FU treatment. Scale bar: 50 μ m. (G) Differentiated cells in lineage-traced RFP⁺ crypts. Villin, MUC2, and CHGA staining depict enterocytes, goblet cells, and enteroendocrine cells, respectively. Stem cells are shown by *LGR5* *in situ* hybridization. Scale bar: 50 μ m. Boxes demarcate first and third quartiles; bars represent median values; tissues were collected 2 days after 5-FU treatment; each dot indicates 1 crypt; individual mice are distinguished by different colors.

mice received dimerizer/doxycyclin treatment and were treated with 5-FU after a 3-day interval, which enabled specific lineage tracing from pre-existing LGR5⁺p27⁺ cells (Figure 5B). After 1 month, the size of clonal ribbons

derived from LGR5⁺p27⁺ cells was significantly larger in the 5-FU-treated xenografts than in untreated controls (Figure 5E and F), which was consistent with the in vitro live imaging data (Supplementary Figure 7C and D) and



suggests the re-acquisition of the proliferative competence after injury. The number of LGR5⁺ cells within the traced BFP⁺ clones also increased after chemotherapy (Figure 5G). These data indicate that LGR5⁺ cells serve as a driver of post-injury regeneration.

Persistence of LGR5⁺p27⁺ Cells Prevents Reversion of KRT20⁺ Cells

Mounting data have supported the model whereby mouse intestinal Lgr5⁺ cells are susceptible to injury and differentiated cells subsequently undergo reversion to replenish lost stem cells.^{6,11,29,30,33} Although our data demonstrate a differing mode of post-injury regeneration in the human intestinal epithelium that emanates from LGR5⁺ cells, it does not exclude the potential contribution of differentiated cells to regeneration. To explore this possibility, we generated LGR5-iCT organoids in which a dimerizer treatment induces apoptosis specifically in LGR5⁺ cells (Figure 6A and B, Supplementary Figure 9A). In LGR5-iCT xenografts, expressions of LGR5-tdTomato and the differentiation marker KRT20 were mutually exclusive (Figure 6C). A treatment with dimerizer efficiently eradicated LGR5⁺ cells, but the engrafts persisted after the ablation (Figure 6C, Supplementary Figure 9B-D). Consistently, proliferating cells were intact during the ablation (Supplementary Figure 9E) and LGR5⁺ cells reappeared by day 15 after the dimerizer treatment (Figure 6C). These results suggest that LGR5-ablated epithelium reserved a proliferating population that could repopulate the crypt bottom.

To determine whether reversion is implicated in post-injury regeneration, we sought to trace non-LGR5⁺ cells using a KRT20-reporter. We introduced KRT20-ERCreER and a Cre-activatable nGFP-BFP reporter into LGR5-iCT organoids (Supplementary Figure 9F and G) and subsequently generated their orthotopic xenografts. Tamoxifen treatment induced expression of the BFP reporter specifically in KRT20-expressing cells in the xenografts (Supplementary Figure 9H). Lineage tracing revealed that the KRT20-lineage diminished over time, confirming their differentiated nature in homeostasis (Figure 6F). Ablation of LGR5⁺ cells by dimerizer treatment allowed KRT20⁺ cells to give rise to LGR5⁺ cells and form clonal ribbon structures, indicative of their de-differentiation capacity (Figure 6G and H). In contrast, lineage formation was not

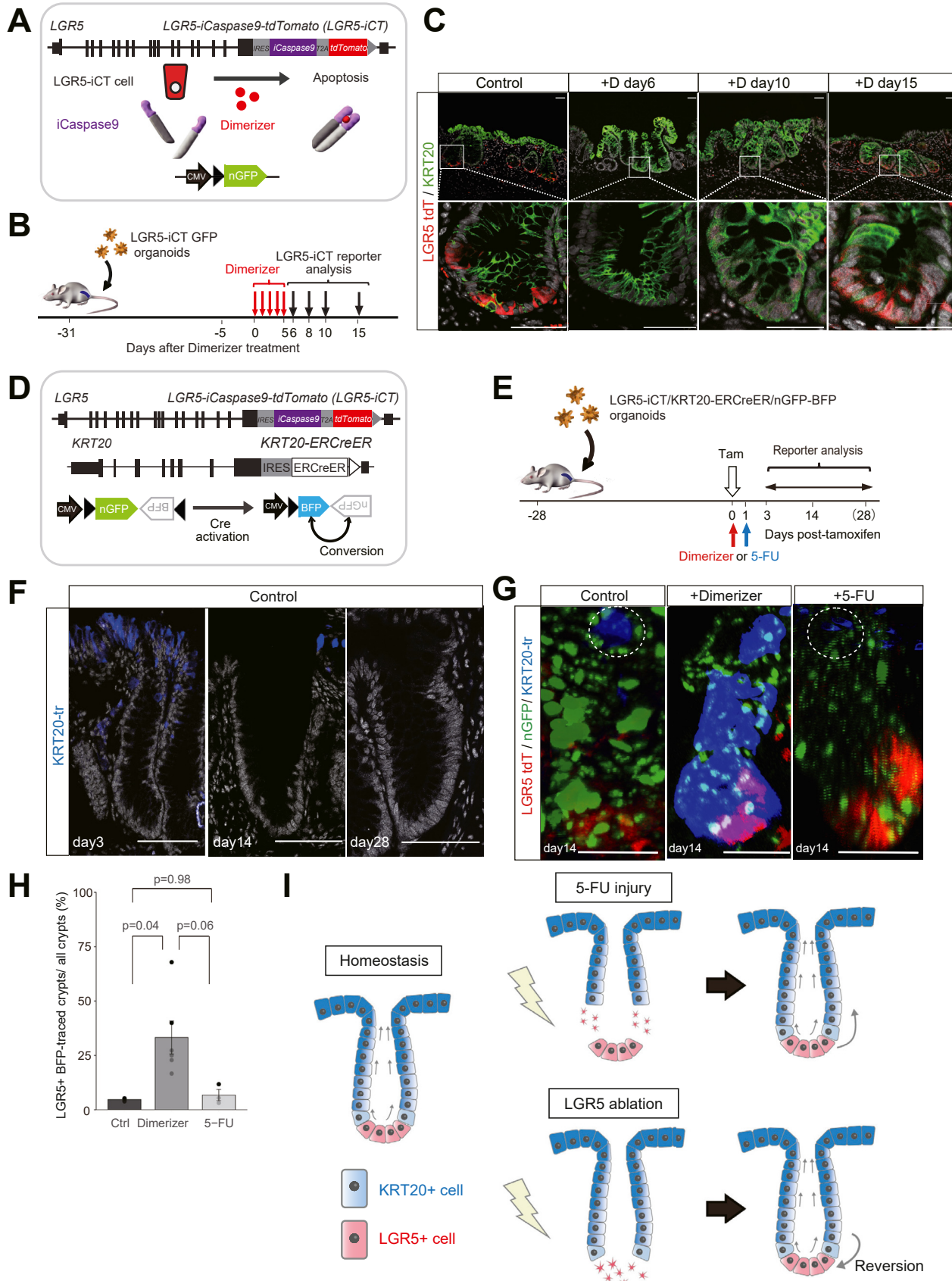
evident after 5-FU treatment, demonstrating the scarcity of reversion events (Figure 6G and H). As shown previously, LGR5⁺ cells persisted at the crypt bottom during 5-FU, and the crypt bottom niche could not be accessed in this situation. Therefore, direct contact with the niche environment may be a prerequisite for KRT20⁺ cells to undergo de-differentiation.

Discussion

We integrated organoid technology, CRISPR-Cas9-mediated genetic knock-in, and orthotopic xenotransplantation to conduct an in-depth functional analysis of LGR5⁺ hCoSCs. By resolving the spatiotemporal restriction of conventional assays, we demonstrated the stemness of slow-cycling LGR5⁺ cells in the human colonic epithelium. Slow-cycling LGR5⁺ CoSCs constitute up to 70% of the LGR5⁺ population in the human colon. An analysis of the EdU incorporation rate in xenografts estimated the cell cycle duration of LGR5⁺p27⁺ stem cells to be 7.3 days. This finding is consistent with identification of LRCs at the human colon crypt bottom using ³H-thymidine pulse chase in the 1960s.^{24,34} Possibly reflecting this dormant state, LGR5⁺p27⁺ stem cells generated small clones in 1-month tracing. Each LGR5⁺ cell-derived clone contained 1.17 LGR5⁺p27⁺ cells, on average (Figure 5G), suggesting that although LGR5⁺p27⁺ cells gave rise to daughter cells in 1 week, only 1 of them could occupy the human crypt stem cell niche throughout the 1-month period. Stated alternatively, LGR5⁺p27⁺ cells rarely gain or lose the stem cell niche. Our results are consistent with the extremely low stem cell replacement rate of 0.65–2.7/year in the human colon, which was estimated by means of spontaneous somatic mutation-based tracing.³⁵ Given the relatively short lifespan of immune-deficient mice, it is challenging to accurately estimate stem cell replacement using xenograft models. Our study also used male mice only, due to the breeder's regulation, and whether the sex of recipient mice affects the cell cycle speed of CoSCs remains unclear. Nevertheless, our results consistently pointed to the substantive difference in stem cell behavior between human and mouse colons.

Inspired by the fact that human colon organoids, but not mouse colon organoids, require TGF- β inhibitor for long-term culture, we explored whether TGF- β signaling contributes to the quiescent state of hCoSCs. An exposure to

Figure 5. In vivo lineage tracing of LGR5⁺p27⁺ cells in homeostasis and tissue injury. (A) Lineage tracing of LGR5⁺p27⁺ cells using the split-Cre system. Heterodimerization of CreC and CreN by means of dimerizer treatment produces functional Cre and enables LGR5⁺p27⁺ cell-specific lineage tracing. (B) Schedule for LGR5⁺p27⁺ split-Cre lineage tracing in orthotopic xenografts. (C) Representative images of a split-Cre xenograft crypt. Fluorescence images of LGR5/p27 tracing (BFP), LGR5-tdTomato, nuclear GFP, and Ki67 immunostaining on 3 days after the last dimerizer are shown. White dotted line outlines a single LGR5⁺BFP⁺ cell that lacks Ki67. n = 18 clones. Scale bars: 50 μ m (left), 20 μ m (right). (D) Stereomicroscopic imaging of a orthotopic xenograft and its 3-dimensional imaging using multi-photon microscopy. Scale bar: 1 mm. (E) Split-Cre xenograft crypts in control and 5-FU-treated mice with small and large LGR5⁺p27⁺ cell clones, respectively. Scale bar: 100 μ m. (F) The size of LGR5⁺p27⁺ cell-derived clones in control and 5-FU-treated xenografts. The difference between the 2 groups was assessed using linear mixed models and likelihood ratio test (P = .013); n = 88 crypts from 5 mice for control, n = 98 crypts from 7 mice for 5-FU. Bars represent median values. Each dot plot represents 1 crypt. Crypts from different individuals are indicated in different colors. (G) The percentage of LGR5⁺BFP⁺ cells per crypt for control and 5-FU. Each dot represents 1 mouse. Welch's t test. P = .01.



COLON

low-dose TGF- β 1 terminated proliferation in human colon organoids but not in mouse organoids. As both human and mouse colon epithelia express TGF β R components, differing regulation downstream of TGF β R may underlie distinct TGF- β sensitivities. A combination of CRISPR-Cas9 and orthotopic xenograft further revealed the increased number of cycling LGR5 $^+$ cells in the TGF β R2-knockout human colon epithelium. These results demonstrated that TGF- β activating microenvironments are operative in the mouse colon, and that epithelium-autonomous TGF- β response controls the cell cycle speed of CoSCs. Although the source of functional TGF- β ligands in the colon remains elusive, reanalysis of the scRNA-seq data revealed the expression of *TGF β 1* in colonic endothelial cells. The observation that a few LGR5 $^+$ p27 $^+$ cells remained in the TGF β R2 knockout colon epithelium also suggests a contribution of other pathways in the cell-cycle regulation of CoSCs.

Our findings recall a long-standing question regarding the species difference, that is, why do human CoSCs exhibit slower cell cycle than mouse counterparts? As the cell division event per se triggers replication errors and tumorigenesis, it is tempting to associate the cell cycle in stem cells with the so-called "Peto's paradox"—large-bodied, long-lived animals should have a greater risk of developing cancer but, in reality, this correlation does not hold true across multiple species.³⁶ Interestingly, a recent study on various animal species has corroborated the relationship between body mass and lifespan and cancer development; larger animals live longer and have less chance of cancer morbidity.³⁷ More recent tour de force genetic analysis has revealed a decreased somatic mutation rate in colon stem cells, along with the increased body size of animals, including humans.³⁸ Taken together, long-lived animals may have experienced an evolutionary force that restrains excessive proliferation of CoSCs to avert tumor development and extend their lifespan. From another perspective based on Peto's thesis, within the same species, larger individuals are at a higher risk of developing cancer. Although it is very interesting to investigate the correlation between body size and cell cycle speed of CoSCs and cancer risk in humans, the cohort size of our study is not sufficient to address this question. We also did not assess the association between the proportion of slow-cycling LGR5 $^+$ cells and other biological backgrounds, such as sex, age, and ethnicity, and more

extensive work will be warranted to clarify the relationship between these factors.

In the mouse intestine, ISCs are eradicated by chemotherapy and replaced with adjacent differentiated cells through de-differentiation.³⁹ In contrast, hCoSCs in the xenotransplanted human colon epithelium persisted during 5-FU treatment and resumed proliferation after treatment cessation. The absence of reversion in 5-FU-induced mucosal injury was not due to the lack of de-differentiation competency, as KRT20 $^+$ differentiated cells still underwent de-differentiation upon genetic ablation of hCoSCs. Thus, our results suggest that the occupancy of hCoSCs in the niche environment restrained the reversion of adjacent differentiated cells. The species difference in the role of stem cells in intestinal regeneration highlights the importance of studying hCoSCs in human-oriented research. Indeed, although several growth factors have been found to facilitate mucosal healing in preclinical mouse models of intestinal injury, none of them has reached clinical translation.^{40,41} Considering the gap between the bench and bedside, building human-relevant experimental strategies will be essential for the development of regenerative therapy for mucosal injury and inflammatory bowel disease.

In conclusion, we identified a slow-cycling subpopulation in human LGR5 $^+$ colonic cells that exerts stemness in homeostasis, and prominently after tissue injury. Although the past decade has seen a certain settlement of the controversy over the existence of reserve stem cells in the mouse intestine,³⁹ our findings illuminated the biological disparities between human and mouse ISCs and emphasized the importance of using human-relevant functional models for accurate understanding of human stem cell dynamics.

Supplementary Material

Note: To access the supplementary material accompanying this article, visit the online version of *Gastroenterology* at www.gastrojournal.org, and at <https://doi.org/10.1053/j.gastro.2022.07.081>.

References

- Weissman IL. Stem cells: units of development, units of regeneration, and units in evolution. *Cell* 2000; 100:157–168.

Figure 6. Kinetics of KRT20 $^+$ cells after LGR5 ablation and mucosal injury. (A) Genetic ablation of LGR5 $^+$ cells in human colon organoids using LGR5-iCaspase9-tdTomato (LGR5-ICT). (B) Schedule for LGR5 ablation experiments. (C) KRT20 immunostaining and LGR5-tdTomato expression in xenografts harvested at the indicated time points. Scale bar: 50 μ m. (D) Genetic design of LGR5-iCT/KRT20-ERCreER organoids. (E) Schedule for KRT20 lineage tracing in xenografts of LGR5-iCT/KRT20-ERCreER organoid. Xenograft-bearing mice were assigned to the control (+tamoxifen [Tam]), LGR5 ablation (+Tam+Dimerizer), or 5-FU treatment (+Tam+5-FU) arm. (F) KRT20-traced clones in the control group. Scale bar: 50 μ m. (G) nGFP expression, KRT20 tracing, and LGR5-tdTomato expression on day 14 in control, dimerizer, and 5-FU groups. Scale bar: 100 μ m. (H) The percentage of crypts with KRT20 $^+$ cell-derived ribbons in all xenograft crypts of control, dimerizer, and 5-FU arms. Welch's *t* test. Data are shown as mean \pm SEM. A dot represents each mouse. $P = .04$ for control vs dimerizer, $P = .06$ for dimerizer vs 5-FU, and $P = .98$ for control vs 5-FU (1-way analysis of variance, followed by Tukey's post-hoc test); 65 crypts from 3 mice (control), 101 crypts from 6 mice (dimerizer), and 86 crypts from 3 mice (5-FU). A proposed mode of human colonic regeneration. Human slow-cycling LGR5 $^+$ cells are injury resistant and show clonogenicity in homeostasis and prominently during regeneration. LGR5-KRT20 $^+$ cells de-differentiate into LGR5 $^+$ cells and undergo clonogenic expansion after LGR5 depletion, but not after mucosal injury, suggesting that regeneration in the human colon epithelium after injury rests on the persistence of slow-cycling LGR5 $^+$ cells rather than the plasticity of KRT20 $^+$ cells.

2. van Velthoven CTJ, Rando TA. Stem cell quiescence: dynamism, restraint, and cellular idling. *Cell Stem Cell* 2019;24:213–225.
3. Post Y, Clevers H. Defining adult stem cell function at its simplest: the ability to replace lost cells through mitosis. *Cell Stem Cell* 2019;25:174–183.
4. Potten CS, Hume WJ, Reid P, et al. The segregation of DNA in epithelial stem cells. *Cell* 1978;15:899–906.
5. Barker N, van Es JH, Kuipers J, et al. Identification of stem cells in small intestine and colon by marker gene Lgr5. *Nature* 2007;449:1003–1007.
6. Asfaha S, Hayakawa Y, Muley A, et al. Krt19(+)/Lgr5(−) cells are radioresistant cancer-initiating stem cells in the colon and intestine. *Cell Stem Cell* 2015;16:627–638.
7. Barriga FM, Montagni E, Mana M, et al. Mex3a marks a slowly dividing subpopulation of Lgr5+ intestinal stem cells. *Cell Stem Cell* 2017;20:801–816.e7.
8. Buczacki SJ, Zecchini HI, Nicholson AM, et al. Intestinal label-retaining cells are secretory precursors expressing Lgr5. *Nature* 2013;495:65–69.
9. Jadhav U, Saxena M, O'Neill NK, et al. Dynamic reorganization of chromatin accessibility signatures during dedifferentiation of secretory precursors into Lgr5+ intestinal stem cells. *Cell Stem Cell* 2017;21:65–77.e5.
10. Tian H, Biehs B, Warming S, et al. A reserve stem cell population in small intestine renders Lgr5-positive cells dispensable. *Nature* 2011;478:255–259.
11. Yan KS, Chia LA, Li X, et al. The intestinal stem cell markers Bmi1 and Lgr5 identify two functionally distinct populations. *Proc Natl Acad Sci U S A* 2012;109:466–471.
12. Yan KS, Gevaert O, Zheng GXY, et al. Intestinal enteroendocrine lineage cells possess homeostatic and injury-inducible stem cell activity. *Cell Stem Cell* 2017;21:78–90.e6.
13. Sato T, Stange DE, Ferrante M, et al. Long-term expansion of epithelial organoids from human colon, adenoma, adenocarcinoma, and Barrett's epithelium. *Gastroenterology* 2011;141:1762–1772.
14. Sugimoto S, Ohta Y, Fujii M, et al. Reconstruction of the human colon epithelium in vivo. *Cell Stem Cell* 2018;22:171–176.e5.
15. Fujii M, Matano M, Toshimitsu K, et al. Human intestinal organoids maintain self-renewal capacity and cellular diversity in niche-inspired culture condition. *Cell Stem Cell* 2018;23:787–793.e6.
16. Oki T, Nishimura K, Kitaura J, et al. A novel cell-cycle-indicator, mVenus-p27K-, identifies quiescent cells and visualizes G0-G1 transition. *Sci Rep* 2014;4:4012.
17. Parikh K, Antanaviciute A, Fawkner-Corbett D, et al. Colonic epithelial cell diversity in health and inflammatory bowel disease. *Nature* 2019;567:49–55.
18. Smillie CS, Biton M, Ordovas-Montanes J, et al. Intra- and inter-cellular rewiring of the human colon during ulcerative colitis. *Cell* 2019;178:714–730.e22.
19. Brugger MD, Valenta T, Fazilaty H, et al. Distinct populations of crypt-associated fibroblasts act as signaling hubs to control colon homeostasis. *PLoS Biol* 2020;18:e3001032.
20. Herring CA, Banerjee A, McKinley ET, et al. Unsupervised trajectory analysis of single-cell RNA-seq and imaging data reveals alternative tuft cell origins in the gut. *Cell Systems* 2018;6:37–51.e9.
21. Hartzell HC, Qu Z, Yu K, et al. Molecular physiology of bestrophins: multifunctional membrane proteins linked to best disease and other retinopathies. *Physiol Rev* 2008;88:639–672.
22. Ritsma L, Ellenbroek SIJ, Zomer A, et al. Intestinal crypt homeostasis revealed at single-stem-cell level by in vivo live imaging. *Nature* 2014;507:362–365.
23. Vlach J, Hennecke S, Amati B. Phosphorylation-dependent degradation of the cyclin-dependent kinase inhibitor p27. *EMBO J* 1997;16:5334–5344.
24. Lipkin M, Sherlock P, Bell BM. Generation time of epithelial cells in the human colon. *Nature* 1962;195:175–177.
25. Potten CS, Kellett M, Rew DA, et al. Proliferation in human gastrointestinal epithelium using bromodeoxyuridine in vivo: data for different sites, proximity to a tumour, and polyposis coli. *Gut* 1992;33:524–529.
26. Hughes KR, Gandara RM, Javkar T, et al. Heterogeneity in histone 2B-green fluorescent protein-retaining putative small intestinal stem cells at cell position 4 and their absence in the colon. *Am J Physiol Gastrointest Liver Physiol* 2012;303:G1188–G1201.
27. Li N, Nakauka-Ddamba A, Tobias J, et al. Mouse label-retaining cells are molecularly and functionally distinct from reserve intestinal stem cells. *Gastroenterology* 2016;151:298–310.e7.
28. Calon A, Lonardo E, Berenguer-Llergo A, et al. Stromal gene expression defines poor-prognosis subtypes in colorectal cancer. *Nat Genet* 2015;47:320–329.
29. Ayyaz A, Kumar S, Sangiorgi B, et al. Single-cell transcriptomes of the regenerating intestine reveal a revival stem cell. *Nature* 2019;569:121–125.
30. Murata K, Jadhav U, Madha S, et al. Ascl2-dependent cell dedifferentiation drives regeneration of ablated intestinal stem cells. *Cell Stem Cell* 2020;26:377–390.e6.
31. Wang Y, Chiang IL, Ohara TE, et al. Long-term culture captures injury-repair cycles of colonic stem cells. *Cell* 2019;179:1144–1159.e15.
32. Yui S, Azzolin L, Maimets M, et al. YAP/TAZ-dependent reprogramming of colonic epithelium links ECM remodeling to tissue regeneration. *Cell Stem Cell* 2018;22:35–49.e7.
33. Tomic G, Morrissey E, Kozar S, et al. Phospho-regulation of ATOH1 is required for plasticity of secretory progenitors and tissue regeneration. *Cell Stem Cell* 2018;23:436–443.e7.
34. Lipkin M, Bell B, Sherlock P. Cell proliferation kinetics in the gastrointestinal tract of man. I. Cell renewal in colon and rectum. *J Clin Invest* 1963;42:767–776.
35. Nicholson AM, Olpe C, Hoyle A, et al. Fixation and spread of somatic mutations in adult human colonic epithelium. *Cell Stem Cell* 2018;22:909–918.e8.
36. Dart A. Peto's paradox put to the test. *Nat Rev Cancer* 2022;22:129.
37. Vincze O, Colchero F, Lemaître JF, et al. Cancer risk across mammals. *Nature* 2022;601:263–267.
38. Cagan A, Baez-Ortega A, Brzozowska N, et al. Somatic mutation rates scale with lifespan across mammals. *Nature* 2022;604:517–524.

39. Shivdasani RA, Clevers H, de Sauvage FJ. Tissue regeneration: reserve or reverse? *Science* 2021; 371:784–786.
40. Krishnan K, Arnone B, Buchman A. Intestinal growth factors: potential use in the treatment of inflammatory bowel disease and their role in mucosal healing. *Inflamm Bowel Dis* 2011;17:410–422.
41. Sandborn WJ, Sands BE, Wolf DC, et al. Repifermin (keratinocyte growth factor-2) for the treatment of active ulcerative colitis: a randomized, double-blind, placebo-controlled, dose-escalation trial. *Aliment Pharmacol Ther* 2003;17:1355–1364.

Received October 13, 2021. Accepted July 19, 2022.

Correspondence

Address correspondence to: Toshiro Sato, MD, PhD, Department of Organoid Medicine, Keio University School of Medicine, 35 Shinanomachi, Shinjuku-ku, Tokyo 160-8582, Japan. e-mail: t.sato@keio.jp.

Acknowledgments

The authors thank the Collaborative Research Resources and JSR-Keio University Medical and Chemical Innovation Center (JKiC), Keio University School of Medicine (T. Tajima from Olympus) for special assistance with ex vivo imaging. The authors thank K. Sugimoto from Yokogawa Electric Corporation for assistance with analysis of *in vitro* live imaging. The authors also thank T. Kitamura for providing the p27-mVenus reporter.

CRediT Authorship Contributions

Keiko Ishikawa, MD (Conceptualization: Equal; Formal analysis: Lead; Investigation: Lead; Methodology: Equal; Software: Equal; Visualization: Lead; Writing – original draft: Lead).

Shinya Sugimoto, MD, PhD (Conceptualization: Equal; Investigation: Supporting; Methodology: Equal; Writing – original draft: Supporting).

Mayumi Oda, DVM, PhD (Formal analysis: Equal; Investigation: Supporting; Software: Equal; Visualization: Supporting).

Masayuki Fujii, MD, PhD (Investigation: Supporting; Writing – review & editing: Equal).

Sirirat Takahashi, PhD (Investigation: Supporting; Visualization: Supporting). Yuki Ohta, MS (Formal analysis: Supporting; Investigation: Supporting; Methodology: Supporting; Software: Supporting).

Ai Takano, PhD (Investigation: Supporting).

Kazuhiro Ishimaru, MD, PhD (Investigation: Supporting).

Mami Matano, MS (Investigation: Supporting).

Kosuke Yoshida, MD (Resources: Supporting).

Hikaru Hanyu, MS (Investigation: Supporting).

Kohta Toshimitsu, MS (Formal analysis: Supporting; Investigation: Supporting; Software: Supporting).

Kazuaki Sawada, PhD (Investigation: Supporting).

Mariko Shimokawa, PhD (Investigation: Supporting).

Megumu Saito, MS (Investigation: Supporting).

Kenta Kawasaki, MD, PhD (Investigation: Supporting).

Ryota Ishii, PhD (Formal analysis: Supporting).

Koji Taniguchi, MD, PhD (Resources: Supporting).

Takeshi Imamura, MD, PhD (Funding acquisition: Supporting; Resources: Supporting).

Takanori Kanai, MD, PhD (Resources: Supporting).

Toshiro Sato, MD, PhD (Conceptualization: Lead; Funding acquisition: Lead; Project administration: Lead; Resources: Lead; Writing – review & editing: Lead).

Data Availability

All data relevant to this study are available from the corresponding authors upon reasonable request. Human RNA sequencing data, single-cell RNA sequencing data, and whole-exome sequencing data were deposited in the DNA Data Bank of Japan database under the accession number JGAS000550 (study) and JGAD000669 (dataset). Mouse single-cell RNA sequencing data were deposited in the National Center for Biotechnology Information under the accession number GSE209649.

Conflicts of interest

This author discloses the following: Toshiro Sato is an inventor on several patents related to organoid culture. The remaining authors disclose no conflicts.

Funding

This work was supported in part by Japan Agency for Medical Research and Development (AMED) CREST grant (JP18gm121001), AMED grants (JP13bm0304001, JP21bm0704069, JP21ek0109523, and JP18gm621008), Japanese Society for the Promotion of Science KAKENHI grant (JP17H06176, JP15K21775, JP20H03758, and JP16H06279), and Keio University Academic Development Funds.

Supplementary Methods

Human Tissues

A healthy human colon sample for scRNA-seq was obtained from a 78-year-old female that underwent elective surgery for ascending colon cancer at Tokyo University Hospital. We had obtained written informed consent following an approval by the ethical committee of the University of Tokyo under ID G3553-(7). Collected tissues were kept in ice-cold phosphate-buffered saline (PBS) until use. Normal colonic organoid lines were previously established from the ascending colon of a 68-year-old female and from the descending colon of a 68-year-old male at Keio University Hospital and Tokyo University Hospital, respectively, with written informed consents.^{1,2} Histopathological sections of healthy human colonic epithelium were obtained as a normal counterpart from six patients undergoing tumor resection. The samples were arbitrarily selected irrespective of the patient's gender, age and body mass index.

Mice

All animal procedures were approved by the Keio University School of Medicine Animal Care Committee. Male NOD/Shi-scid, IL-2R γ ^{null} (NOG) mice (5-6 weeks old)³ and C57BL/6 wild-type mice were obtained from the Central Institute for Experimental Animals (CIEA, Japan) and housed under specific pathogen-free conditions. Removal of the mouse colonic epithelium and subsequent orthotopic xenotransplantation of human colonic organoids were carried out as previously described.²

Crypt Isolation and Organoid Culture

We performed crypt isolation and cultured human colonic organoids as previously described.⁴ Briefly, the underlying stroma was trimmed from the tissues using sharp forceps, and the epithelium was further shed into small fragments of around 1 mm³ in size. Sheared epithelium was further washed with ice-cold PBS at least five times and gently rocked in 2.5 mM EDTA (Thermo Fisher Scientific) in PBS for 1 hour at 4°C on a shaker. Crypts were isolated by repeated pipetting and centrifuged at 200 × g for 3 min. The crypt palette was suspended in Matrigel (Corning) on ice. Crypt-laden Matrigel was dispensed onto 48-well culture plates and following solidification of Matrigel droplets, the crypts were overlaid with the following medium: Advanced Dulbecco's Modified Eagle's Medium/F12 (Thermo Fisher Scientific) supplemented with penicillin/streptomycin (Thermo Fisher Scientific), 10 mM HEPES (Thermo Fisher Scientific), 2 mM GlutaMAX (Thermo Fisher Scientific), 1× B-27 Supplement (Thermo Fisher Scientific), 10 nM gastrin I (Sigma-Aldrich), 1 mM N-acetylcysteine (FUJIFILM Wako Pure Chemical), and the niche factors of 100 ng/ml recombinant mouse Noggin (Pepro-Tech), 50 ng/ml recombinant mouse EGF (Thermo Fisher Scientific), 100 ng/ml recombinant human IGF-1 (Bio-Legend), 50 ng/ml recombinant human FGF-basic (FGF-2) (PeproTech), 10% R-spondin1 conditioned medium, 500

nM A83-01 (Tocris) and 20% Afamin-Wnt-3A serum-free conditioned medium⁵ as previously reported.⁴ Organoids were passaged weekly at a 1:10 split ratio by single cell dissociation using TrypLE Express (Thermo Fisher Scientific). We added 10 μM Y-27632 (FUJIFILM Wako Pure Chemical) for the first 2 days after passaging to prevent anoikis. TGF-β activation in organoids was done by treating organoids with either 0.1 or 1 ng/ml TGF-β1 (R&D) for 24 hours in an A83-01-free condition. Mouse colonic organoids were established from 12-week-old Lgr5-DTR-EGFP mice (a kind gift from F.J. de Sauvage) using the same method as described above. To exclude the effect of culture condition, the culture media for human organoids supplemented with N2 supplement (Thermo Fisher Scientific) was used to maintain mouse colonic organoids.

Gene Engineering of Organoids

We generated *LGR5-tdTomato*, *LGR5-iCaspase9-tdTomato* (*LGR5-iCT*), *LGR5-CreERT2*, *LGR5-NLS-split-Cre* and *KRT20-ERCreER* knock-in (KI) organoids as previously described.⁶ The 20-bp single guide RNA (sgRNA) target sequences were cloned into the px330-U6-Chimeric_BB_CBh-hSpCas9 plasmid (Addgene #42230) for the generation of LGR5-specific sgRNA. Donor vectors of the LGR5 and KRT20 reporters were generated as follows. The *LGR5-GFP* and *KRT20-GFP* vector was first generated by cloning PCR-amplified 5' and 3' homology arms into the *Ires-GFP-loxP-pEF1α-RFP-T2A-puro-loxp* plasmid (HR180PA-1, SBI) using In-Fusion HD Cloning kit (Clontech). The *GFP* cassette of this vector was replaced with *tdTomato*, *iCaspase9-T2A-tdTomato*, *CreERT2* and *NLS-FKBP-F2-Cre60-343* for the assembly of *LGR5-tdTomato* KI, *LGR5-iCT* KI, *LGR5 /KRT20-CreERT2* KI and *LGR5-NLS-split-CreC* KI, respectively.

The split-Cre system was designed as reported previously.^{7,8} Two fragments of Cre, namely CreN and CreC, derived from Cre codons 19–59 (N-terminal) and 60–343 (C-terminal), respectively. Each Cre fragment was fused to the FKBP (F36V) domain by F2 linkers, such that dimerization of the two Cre fragments by dimerizer (AP20187, Clontech) led to the activation of Cre. CreC was synthesized as *NLS* (*nuclear localization signal*)-FKBP (F36V)-F2-CreC with flanking *NheI* sites for ligation and was cloned into the *LGR5-KI* vector. CreN was synthesized as *p27^k-F2-FKBP(F36V)-F2-CreN*. This cassette was introduced into the XLone-GFP plasmid (Addgene #96930) by replacing the GFP cassette using TAKARA Ligation kit ver.2.1 (Clontech). The sequences of CreN and CreC are available on request.

For visualization of p27, we cloned the *p27-mVenus* reporter (a gift from T. Kitamura, The University of Tokyo) into a PiggyBac vector (PB533A-2, SBI). The *nGFP-BFP* reporter was obtained by cloning *nGFP-T2A-puro* and inverse *TagBFP2* cassettes flanked with *loxP* sites into a PiggyBac vector (PB510B-1, SBI). The *iRFP-BFP* reporter was made by replacing *nGFP* with *iRFP*. The constitutive *TagBFP2* expression vector was made by cloning a synthesized *TagBFP2* cassette into a PiggyBac vector (PB510B-1, SBI).

Gene reporter and CRISPR vectors were introduced into human normal colonic organoids using electroporation as reported previously⁹ with slight modifications. The electroporated organoids were incubated at 30°C for 2 days to induce cold shock,¹⁰ followed by a 2-day selection with 2 µg/ml puromycin (Thermo Fisher Scientific) from 5 days after electroporation. Puromycin-resistant clones were manually picked up and expanded for PCR-based genotyping. The puromycin-RFP cassette flanked by *loxP* was subsequently deleted by a transient transfection of organoids with Cre-expressing adenovirus (TaKaRa) at a multiplicity of infection of 0.3. RFP-deficient-clones were manually picked up, and deletion of the puromycin-RFP cassette was confirmed by genomic PCR. *p27-mVenus* clones were selected with 100 µg/ml Geneticin (Thermo Fisher Scientific) for human and mouse organoids for 1 week. After generation of *LGR5-iCT p27-mVenus* clones, the *CreERT2* cassette was knocked-in to the intact *LGR5* allele, followed by the electroporation of the *iRFP-BFP* vector. In parallel, *LGR5-iCT p27-mVenus* organoids were labeled with the BFP-puro PiggyBac Vector for the visualization of the xenotransplanted area. We also used *LGR5-CreERT2* rainbow organoids generated in the previous study.²

Split-Cre organoids were generated by the knock-in of *NLS-FKBP-F2-CreC* to the intact *LGR5* allele of *LGR5-tdTomato* organoids, followed by the electro-transfer of *XLone-p27-F2-FKBP-F2-CreN* and *nGFP-BFP* vectors. Organoids with the expression of XLone reporters were selected by 1-week treatment with 5 µg/ml of Blasticidin S (FUJIFILM Wako Pure Chemical). For dimerization of split-Cre, organoids were treated with 250 ng/ml doxycycline (Thermo Fisher Scientific) overnight 3 days after passaging and washed with PBS at least 3 times. Four days after doxycycline treatment, we treated the organoids with 500 nM dimerizer overnight. The sequences of *LGR5* and *KRT20* sgRNAs and primers for genomic DNA used in this study are shown in Supplementary Table 1.

Sample and Library Preparation for scRNA-seq

An ascending colon tissue derived from a 78-year-old female was used for droplet-based scRNA-seq. Following sampling from a surgically resected specimen, the tissue was immediately placed into ice-cold PBS and transferred to the laboratory. The submucosal tissue was trimmed off with fine scissors and the mucosal layer was cut into small pieces of around 1 mm³ in size. The sample was treated with 2.5 mM EDTA for 60 min at 4°C on a rocking shaker, and crypts were released by pipetting. Single cells were obtained by treating crypts with TrypLE Express for 5 min at 37°C and by subsequent filtering through a 20-µm cell strainer. For purification of epithelial cells and removal of dead cells, the cells were suspended in 200 µl of cold PBS and stained with 5 µl of an APC anti-human CD326 (EpCAM) antibody (324208, BioLegend) and with DAPI (BD Biosciences, 1:1000) for 20 min, and live EpCAM⁺ single cells were sorted into a 1.5-mm tube using a cell sorter (SH800, Sony). The cells were spun down and suspended in 1% bovine serum albumin in PBS. Cell density was measured using

Countess II Automated Cell Counter (Thermo Fisher Scientific), and a total of 17,000 cells were subjected to library construction. Library construction was performed using Chromium Single Cell 3' Reagent Kit (v2) and a Chip Kit (10x Genomics) according to the manufacturer's instructions. Sequencing was outsourced (BGI), and the library was sequenced using a HiSeq4000 sequencer (Illumina) with 100 bp paired-end reads and with 30% of PhiX Sequencing Control (Illumina) spike-ins for quality control. For scRNA-seq of the mouse colonic epithelium, we isolated mouse colonic crypts from 3 female 12-week-old C57BL/6 mice. For purification of epithelial cells and removal of immune cells and dead cells, the cells were suspended in 200 µl of cold PBS and stained with 5 µl of APC anti-mouse CD326 (EpCAM) antibody (118213, BioLegend), PE anti-CD45 antibody (BD Biosciences, 1:500) and DAPI (1:1000) for 20 min. Live CD45⁻ EpCAM⁺ single cells were sorted into a 1.5 mm tube using a cell sorter. A single-cell library was generated following the procedures used for human tissue.

Data Processing for scRNA-seq

The sequence read data from human colonic epithelial cells was mapped onto the human genome (GRCh38) using CellRanger (version 3.0.2) (10x Genomics). CellRanger detected 8709 cells and 33,538 features from our human colonic epithelial sample. The count data was imported into the R package Seurat (version 4.0.3).¹¹ We filtered out cells with less than 1000 or more than 8000 unique genes, and those with mitochondrial unique molecular identifier (UMI) counts over 20%. Finally, we obtained the expression data of 33,538 features in 7103 cells. After filtration, the median detected feature was 3148.

The data from mouse colonic epithelial cells was mapped onto the mouse genome (GRCm38) using CellRanger. 3638 cells with 31,053 features were obtained. After filtering out cells with less than 1000 and more than 8000 genes and those with mitochondrial UMI counts over 20%, 1260 cells with the median detected feature of 4447.5 were retained.

Clustering and Identification of Cell Type Signatures

The count data of human colonic epithelial cells was normalized and scaled using SCTtransform¹² and Gamma-Poisson generalized linear models.¹³ Principal component analysis (PCA) was performed using top 3000 variable genes, followed by uniform manifold approximation and projection (tSNE) using top 30 principal components. An SNN graph was constructed using top 30 principal components with the FindNeighbors function, and the cells were classified using the FindClusters function with the resolution parameter 0.5. This step clustered the cells into 10 clusters. To characterize each cluster, we performed differentially expressed gene (DEG) analysis using the FindAllMarkers function with the RNA assay. From the gene expression pattern, we assigned the clusters to early/late colonocytes, goblet/immature goblet cells, BEST4/OTOP2

cells, secretory progenitor cells, 3 transient amplifying cell populations (TA-1, TA-2 and TA-3) and LGR5⁺ stem cells. Their RNA assay data was also normalized and scaled by Seurat for plotting. DEG analysis of the stem cell and early progenitor subtypes (Stem, TA-1/2/3 and Secretory progenitor) was performed using FindAllMarkers. The thresholds of adjusted *P* value = 0.01 and mean log₂ fold-change = 0.6 were used. The cell cycle score was calculated with the CellCycleScoring function using S and G₂M genes reported previously.¹⁴ The ISC score was calculated with the PercentageFeatureSet function using *LGR5*, *ASCL2*, *SMOC2*, and *AXIN2* genes. The abundance of mouse (Mm) LRC and Mex3a signatures genes¹⁵ in each cell was also calculated with the PercentageFeatureSet function. From the mouse intestinal LRC signature and Mex3a-enriched genes, we used 62 and 208 genes that had human orthologues, respectively.

Integrative scRNA-seq Analysis Using Public Datasets

A single-cell gene expression dataset of the human colon¹⁶ was downloaded from Gene Expression Omnibus under the accession code GSE116222. We analyzed 4249 cells from 3 healthy subjects (A1, B1, C1). Another single-cell gene expression data of the human colon¹⁷ was downloaded from Single Cell Portal under the accession code SCP259. The data by Smillie et al included 49,757 colonic epithelial cells from 12 healthy subjects. To balance the size with the other datasets, we selected 5557 epithelial cells from 4 healthy subjects (N16.EpiA, N18.EpiB, N20.EpiB and N21.EpiB). We filtered out cells with less than 500 and more than 8000 unique features, and those with mitochondrial UMI counts over 30% and obtained data of 4244 and 3457 human colonic epithelial cells from these data. The medians of detected features were 1451 (Parikh et al) and 1531 (Smillie et al).

Integrative analysis was performed based on the data integration framework in the R package Seurat (version 4.0.3).¹⁸ Each dataset was normalized with SCTtransform, and passed to the PrepSCTIntegration function using the 2000 integration features selected by the SelectIntegrationFeatures function. The integration anchors were extracted by the FindIntegrationAnchors function and used for data integration using SCT as a normalization method. PCA was performed using top 2000 variable genes, and UMAP was performed using top 20 principal components. An SNN graph was constructed using top 20 principal components with the FindNeighbors function, and the cells were classified using the FindClusters function with the resolution parameter 0.7.

Comparison of Human and Mouse scRNA-seq Data

To compare the human and mouse scRNA-seq data, we first obtained public scRNA-seq datasets of the mouse colon and colonic epithelial cells^{19,20} from GEO database under accession codes GSM4569728 and GSM2743164, respectively, to increase the number of mouse cells. Our human

and mouse data and the two public mouse scRNA-seq datasets were integrated as we did for the human scRNA-seq datasets, with some modifications. The feature names in the mouse data were capitalized to match with the feature names in human data, and we regressed out the percent mitochondrial UMI counts and the number of detected features in the second non-regularized linear regression of SCTtransform.

We performed PCA, followed by UMAP clustering using top 20 principal components. Of the 7496 mouse cells in Brugger et al data and 1739 in Herring et al, we extracted 2706 and 1736 cells, respectively, with a membership in the *Epcam*-positive cluster. By filtering out cells with less than 500 or more than 8000 detected genes and those with mitochondrial RNA proportion above 25%, we obtained 1404 and 655 mouse colonic epithelial cells with median detected features of 2383 and 3186 from Brugger et al and Herring et al datasets, respectively.

Orthotopic Xenotransplantation of Human Colonic Organoids

Removal of the mouse colonic epithelium and subsequent orthotopic xenotransplantation of human colonic organoids were carried out as previously described.² Male NOG mice (7–10 weeks) were fed with a normal diet and housed in a room with a regular 12-hour light cycle (8:00–20:00 light, 20:00–8:00 dark). Before the xenograft experiment, mice were allowed to produce as much feces as possible while running around in the cage by a long-term inhalation of 1.5–2% isoflurane. For the removal of the mouse colonic epithelium, the mouse colonic lumen was washed with PBS for the removal of luminal contents and debris using a thin catheter (flexible animal feeding needle, Fuchigami). We inserted a hand-made thin catheter (1 mm in diameter) with a small balloon at the tip into the mouse anus. The colonic mucosa was infused with hot EDTA (250 mM, 50–55°C) using another catheter for 2–3 minutes and by closing the oral and anal ends of the rectum with the inflated balloon and tweezers (HSC702-93; Hammacher), respectively. The lumen was washed with PBS, followed by the decanulation of the balloon-tipped catheter. We then removed the native colonic mucosa by scraping the epithelium off the colonic wall with a vibrating electric toothbrush (EW-DL22, EW0945; Panasonic Corporation). Specifically, the brush tip was inserted into the distal colon from the anus and gently pressed onto the inner surface of the lumen wall, allowing crypts to be mechanically rubbed off from the submucosal layer. Successful removal of crypts was confirmed as a release of isolated crypts from the vibrating toothbrush into a water-filled petri dish. The balloon-tipped catheter was inserted again to wash the lumen with PBS.

Orthotopic xenotransplantation of human colonic organoids labelled with fluorescent reporters was performed within 2 hours after the removal of the colonic epithelium in recipient mice. Before engraftment, the organoids were grown in suspension culture for 3–4 days after single-cell passaging using the culture medium supplemented with 2-

2.5% (vol/vol) Matrigel and ultra-low attachment 6-well culture plates (Corning). Following a rough estimation of total cells in organoids by cell counting, the organoids were suspended in PBS supplemented with 10% (vol/vol) Matrigel, and 70 μ l of the organoid suspension containing 1×10^6 cells was injected into the recipient colon using a 200 μ l pipette. To temporarily maintain the transplanted organoids in the colon, we covered the anus of mice with an adhesive (AronAlpha 31303; Toagosei) and a small piece of soft paper, which was manually removed 3–6 hours after transplantation. We carefully monitored defecation from recipient mice for 1 week to check for the occurrence of bowel obstruction. In total, 6 organoid lines with fluorescent reporters were xenotransplanted orthotopically and analyzed in this experiment.

Mouse Colonoscopy

Successful orthotopic engraftment of organoids was confirmed by endoscopy as previously described.² Briefly, the fluorescence of engrafted organoids was observed > 14 days after transplantation using a high-definition 3-charge coupled device camera system (Image 1 Hub HD H3-Z; Karl Storz) and 300 Watt Xenon light source (D-Light C; Karl Storz). The camera-tipped-HOPKINS telescope (1.9 mm outer diameter, length 10 cm; Karl Storz) was inserted and guided into the recipient mouse rectum via transanal approach after a removal of remnant stools. Endoscopic images were filmed and recorded in both bright field and fluorescence imaging. We considered orthotopic xenotransplantation to have succeeded when fluorescence-expressing areas were evident > 28 days after transplantation. To measure the xenograft area at multiple time-points after dimerizer treatment, we inserted a biopsy forceps (61071ZJ; Karl Storz) into the mouse rectum through the working channel of the colonoscopy and used its size as the reference area in bright field. Then, fluorescent GFP⁺ areas were filmed from the closest approaching location at the indicated time points. The measurement of the GFP⁺ area was done using the Fiji (ImageJ) software.

Mouse Drug Treatment

Each mouse was euthanized around the same time in a day to minimize the adverse effect of circadian rhythms on the proliferation state.²¹ For the LRC experiments, each mouse was continuously treated with EdU (10 mg/kg; Thermo Fisher Scientific) intraperitoneally every 8 hour over 4 days, and the tissues were assessed on 0.5, 14, 21, and 28 days after last EdU treatment. Mucosal injury was induced by 2 rounds of daily intraperitoneal injection of 100 mg/kg 5-FU (Kyowa Kirin). Donor human crypts and recipient mouse crypts were assessed in the same mice. In lineage tracing experiments, each mouse received a single intraperitoneal injection of 0.5 mg tamoxifen (Sigma-Aldrich) diluted in 200 μ l corn oil and treated with a single 150 mg/kg 5-FU treatment on 3 days after tamoxifen injection, because 3 days were required for the recombination and visualization of rainbow-expressing cells.² For LGR5 p27 split-Cre tracing in vivo, p27 CreN expression was

induced by a 6-day treatment with 1 mg/ml doxycycline in drinking water. The 2 Cre fragments were dimerized by at least 3 rounds of daily intraperitoneal treatment with 250 μ g of dimerizer. Mucosal injury was induced by a single intraperitoneal injection with 150 mg/kg 5-FU on 3 days after the last dimerizer injection. Day 0 was defined as the day of the 5-FU treatment and split-Cre-traced tissues were analyzed on day 0 and day 28. For LGR5 ablation experiments, xenograft-bearing mice received 40 μ g of dimerizer for 5 consecutive days. For LGR5-iCT/KRT20-ERCreER lineage tracing experiments, each mouse received a single intraperitoneal injection of 0.5–2 mg tamoxifen (Sigma-Aldrich) diluted in 200 μ l corn oil. The mice were treated either with a single 150 mg/kg 5-FU treatment on the following day after tamoxifen injection or with a single 100 μ g of dimerizer on the same day as tamoxifen injection. Xenograft tissues were analyzed on day 3, 14, and 28 for control, on day 14 for dimerizer and 5-FU treatment groups.

Organoid Whole-mount Staining

Human colonic organoids were grown for 5–7 days after single-cell passaging for whole-mount staining. The organoids were isolated from Matrigel using Cell Recovery Solution (Corning) for 30 min on ice and fixed in 4% PFA for 20 min at room temperature. The organoids were washed with PBS 3 times, blocked with 10 \times diluted Power Block Universal Reagent (BioGenex) at room temperature for 10 min, and reacted with a primary antibody in the permeabilization buffer (0.2% Triton-X-100 in PBS) on a shaking rocker at 4°C overnight. The organoids were washed with PBS 3 times and labelled with a secondary antibody at room temperature for 30 min and with Hoechst 33342 (Thermo Fisher Scientific) for nuclear counter-staining. Stained organoids were suspended in ProLong Diamond Antifade Mountant (Thermo Fisher Scientific), mounted onto a 35-mm glass bottom dish and observed using a confocal microscope (SP8, Leica). Primary and secondary antibodies used in this experiment were as follows: mouse anti-p27 (F-8) (1:200; sc-1641, Santa Cruz Biotechnology), rabbit anti-Ki67 (1:100; ab16667; Abcam), and Alexa 488, 568, 647-conjugated anti-rabbit or anti-mouse antibody (1:200; Thermo Fisher Scientific).

Tissue Immunohistochemistry, Immunofluorescence and In Situ Hybridization

The preparation of samples from mouse or colon xenograft tissue for immunofluorescence or immunohistochemistry was carried out by fixation in 4% paraformaldehyde (PFA) for 6–18 hours, followed by the trimming of fluorescence-labelled donor human colonic crypts under a stereomicroscope (Nikon, Lumina Vision). The tissues for immunofluorescence staining were immersed in 30% sucrose overnight and subsequently embedded in OCT compound (Tissue-Tek). For cryosectional analysis, the tissues were sectioned with an 8 μ m thickness. For tissue whole-mounting and 3-dimensional imaging, the donor human colon tissues after penetration of sucrose were submerged in the tissue-clearing-fluid LapiClear 1.49 (SUNJin Lab Co.) for

2–3 days with gentle shaking. Paraffin-embedded tissues were sectioned with 4 μm and 7 μm thicknesses for immunohistochemistry and *in situ* hybridization, respectively. For immunostaining, the following primary antibodies were used: rabbit anti-Ki67 (1:100; ab16667; Abcam), rat anti-Ki67 (SolA15) (1:100; 14-5698-82; Thermo Fisher Scientific), rabbit anti-p27 (1:100; ab32034; Abcam), mouse anti-p21 (F-5) (1:100; sc-6246; Santa Cruz Biotechnology), rabbit anti-p57 (1:500; P0357; Sigma), rabbit anti-RFP (1:500; PM005; MBL), mouse anti-KRT20 (Ks20.8) (1:50; M7019; Dako), rabbit anti-Mucin2 (H-300) (1:100; sc-15334; Santa Cruz Biotechnology), goat anti-Villin (C-19) (1:100; sc-7672; Santa Cruz Biotechnology), goat anti-Chromogranin A (C-20) (1:100; sc-1488; Santa Cruz Biotechnology), mouse anti-Chromogranin A (C-12) (1:100; sc-393941; Santa Cruz Biotechnology), goat anti-GFP (1:200; ab6673, Abcam), rabbit anti-Cleaved Caspase-3 (1:100; 9661, Cell Signaling), rabbit anti-SMAD3 (phospho S423 + S425) (EP823Y) (1:20; ab52903; Abcam), and rabbit anti-tagRFP (1:1000; Evrogen). Alexa 488-, 568-, 647-conjugated anti-rabbit, -mouse, -goat antibodies (1:200; Thermo Fisher Scientific) were used as secondary antibodies. Nuclear counterstaining was performed using Hoechst 33342 (1:1000; H3570; Thermo Fisher Scientific). For EdU detection was done using the Click-iT Plus EdU Imaging Kit (Thermo Fisher Scientific). *In situ* hybridization was performed using the RNAscope 2.5HD kit (Advanced Cell Diagnostics) according to the manufacturer's protocol. We used cryosections for the analysis of lineage tracing and paraffin-embedded sections for all the other analyses, respectively. The probes used in this study were human *LGR5* probe (311021), mouse *Lgr5* probe (312171), and positive (*PPIB*) and negative (*DapB*) control probes. The sections were visualized using an SP8 confocal microscope (Leica) or a BZ-X800 digital microscope (Keyence). Images were analyzed using Fiji.

Confocal Counting Experiments

The status of Ki67 in LGR5⁺ or Lgr5⁺ cells following 5-FU-induced injury was assessed by counting the number of Ki67⁺ and LGR5⁺ cells in donor human crypts and recipient mouse crypts. In LRC experiments, LRC was defined as EdU⁺ cell located between the crypt bottom and the 10th cellular position from the crypt base at the indicated time points, and the numbers of LGR5 (Lgr5)⁺ cells and LGR5⁺ EdU⁺ cells were counted manually in each crypt at each time point. In section analyses, we excluded slantly sectioned crypts, specifically the crypts that did not have a typical U-shape. A uniform laser intensity was used in each assessment. In LGR5-p27-LRC reporter experiments, LGR5⁺ (tdTomato) cells, p27⁺ (mVenus) cells, and LRCs were counted up to the 10th position from the crypt bottom. The expression of the LGR5 and p27 reporters was analyzed using the 3D object Counter plugin in Fiji.

Flow Cytometry and Colony Forming Efficiency Analysis

For the analysis of organoid formation from single cells, LGR5-p27-reporter organoids grown for 5 days after

passaging were dissociated into single cells in TrypLE Express at 37°C for 25 min and filtered through a 20- μm cell strainer (Partec). The cells were washed with PBS and stained with DRAQ7 (Biostatus) to mark dead cells. The cells were analyzed and sorted using a flow cytometer with a 100- μm sorting chip (FACS SH800, SONY). Single cells were gated based on the SSC-H versus SSC-W profile. The fluorescence of p27-mVenus, LGR5-tdTomato and DRAQ7 was excited using 488 nm, 561 nm, and 638 nm using 525/50, 617/30 and 665/30 bandpass filters, respectively. We used single-colored organoids (namely, tdTomato-expressing organoids and mVenus-expressing organoids) and control organoids for the fluorescence compensation of p27-mVenus and LGR5-tdTomato. The gated cells (10 cells per gate) were sorted onto slides, and the correct fluorescence was confirmed by confocal microscopy. For each cell population, 1000 cells or 2000 cells were sorted and seeded in a 20 μl droplet of Matrigel per well. The culture medium was supplemented with 10 μM Y-27632 for the first two days. Images were captured on day 5 and day 7 post sorting using a BZ-X800 digital microscope (Keyence). Colony numbers and total colony areas were measured using the BZ-X800 analyzer software (Keyence). Three or 4 replicates were generated for each of the 2 independent LGR5-tdTomato lines.

In vitro Live Imaging

Human organoids for *in vitro* live imaging were plated in 10 μl of Matrigel on a 96-well plate (IWAKI). The growth medium was refreshed every 3 days, and the organoids were treated with 10 μM 5-FU for 1 day and washed with PBS at least 3 times where indicated. Wells in the outer 2 rows and columns of the plates were not used for imaging to minimize the fluctuations in laser intensity, temperature and humidity, and were filled with PBS to prevent medium evaporation. Organoids were maintained at 37°C and 5% CO₂ for the indicated days using a stage-top incubator. Time-lapse *in vitro* live imaging was carried out using an inverted confocal quantitative image cytometer CQ1 (Yokogawa Electric Corporation). BFP, p27-mVenus, LGR5-tdTomato, and iRFP were excited using 405 nm, 488 nm, and 561 nm, and 640 nm lasers and collected using 447/60, 525/60, 617/73, and 685/40 nm band pass filters, respectively. A 20 \times dry objective lens (NA 0.75) was used to capture high-resolution fluorescence images. The images in the indicated areas were captured every 8 hours over 4 consecutive days for the observation of nonperturbed organoid growth, and every 12 hours over 14 days for 5-FU experiments. Z-stack images were filmed at 3–5 μm depth intervals for each organoid. Cell tracking analysis and graphing were performed automatically using the Cell-Pathfinder CQ1 software (Yokogawa Electric Corporation). Nontrackable cells and the cells that showed dynamics inconsistent with the manual time tracking results were excluded from the analyses. For mouse Lgr5-GFP/p27-mVenus organoids, live imaging was performed on a confocal microscope (SP8, Leica) because CQ1 could not separate the wavelength of Venus from that of GFP. Lgr5-

GFP and p27-mVenus were excited using 488 nm and 514 nm lasers. A 20 \times dry objective lens (NA 0.75) was used to capture high-resolution fluorescence images.

Three-dimensional Ex Vivo Imaging and Counting Experiments

Transparent tissue specimens in LapiClear 1.49 were placed onto 35-mm glass base dishes (IWAKI) and mounted with a 18-mm micro cover slip (Matsunami Glass) on glue. The dish was placed upside down with water poured onto the backside of the dish bottom. Fluorescence 3D imaging was performed using an upright multiphoton laser scanning microscope system A1R MP+ with GaAsP NDD (Nikon). Tag BFP2, nuclear GFP and tdTomato were excited with 820 nm, 900 or 960 nm, and 1040 nm lasers and collected with < 498 nm, 498–560 nm and 560–593 nm fluorescein filters, respectively. To eliminate the signal of second harmonic generation (SHG) from Tag BFP2 images, < 498 nm-filtered images on 900 nm emission was subtracted from < 498 nm-filtered images on 820 nm emission. Z-stack images were captured at a 3 μ m interval. The images were median-filtered, merged and 3D-reconstructed using the Fiji software. We considered that when 2 given BFP-expressing cells were located more than 10 cells apart from each other, they were derived from different BFP $^+$ clones. BFP-expressing cells localized to the crypt top and did not extend from the crypt bottom or LGR5-tdTomato cells were excluded from the analysis.

RNA-sequencing

RNA was extracted from organoids using the RNeasy Plus Mini Kit (Qiagen). RNA quality was measured using Agilent 2100 Bioanalyzer (Agilent), and all samples passed the quality check (RNA Integrity Number > 7.0). Sequence library was prepared with TruSeq RNA Library Prep Kit v2 (Illumina) and sequenced with HiSeq 4000, NovaSeq 6000 or HiSeq X Ten (Illumina). RNA sequencing was outsourced to GENEWIZ. Adaptors were removed from raw fastq files with cutadapt (version 1.18) and the reads were aligned to hg38 using STAR (version 2.6.1). The expression levels of the human genes in Ensembl release 81 were estimated with RSEM (version 1.3.3). The concordance of the gene expression profiles across the organoids was assessed as the Pearson's correlation of log₁₀(TPM + 0.001) values of all genes.

Exome Sequencing

Genomic DNA was extracted from organoids using the QIAamp DNA Blood Mini Kit (Qiagen) and was treated with RNase Cocktail (Ambion). Three micrograms of genomic DNA were subject to whole exome sequencing. 150 bp paired-end libraries were prepared using the SureSelect Human All Exon V6 kit (Agilent) according to the manufacturer's instructions. Cleaned fastq files were mapped onto the human reference genome version GRCh37 (hg19) using BWA-MEM (version 0.7.17). Data cleanup and variant detection were performed using Genome Analysis Toolkit

(GATK, version 4.1.2.0). PCR duplicates were marked, and then base quality score recalibration was applied. Variant detection was performed using Mutect2. To remove germline variants, the detected variants were filtered by removing those detected with allele frequency of 0.1% or more in dbSNP or the Japanese germline variant database (the Human Genetic Variation Database).²² Genotypes of 53,867 exonic germline variants registered in HapMap (version 3 release 3) were compared using Cross-checkFingerprints (GATK version 4.1.2.0).

Real-time Quantitative PCR

Total RNA was extracted from organoids using RNeasy Mini Kit (Qiagen) and cDNA was synthesized using High Capacity RNA-to-cDNA kit (Thermo Fisher Scientific). qPCR was carried out using Universal Probe Library probes and FastStart Essential DNA Probes Master (Roche) on a Light-Cycler 96 device (Roche). Relative gene expression levels were analyzed by delta-delta CT method using ACTB as a house keeping gene.

Mathematical Estimation of Cell Cycle Length

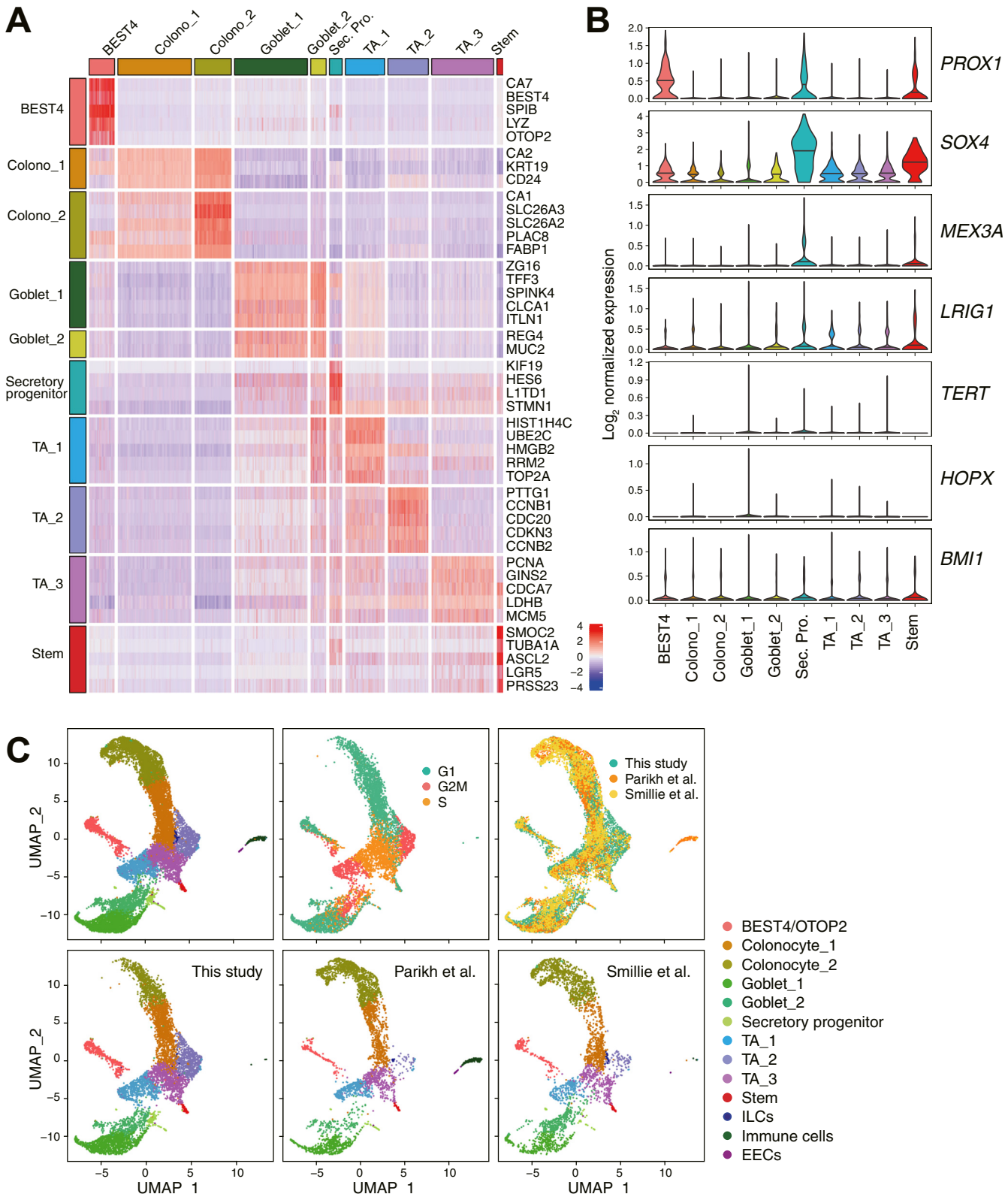
To estimate the cell cycle length in the non-dividing LGR5 $^+$ subpopulation and LGR5-expressing TA cells, we counted the frequencies of EdU $^+$ cells in all LGR5 $^+$ cells on days 0.5, 14, and 21 after an EdU pulse. As LGR5 $^+$ Ki67 $^+$ cells (LGR5 $^+$ p27 $^+$ cells) were distributed around the +0 to +4 cell position (Figure 1E) in native human colon crypts, we measured the frequency of EdU $^+$ LGR5 $^+$ cells in +0 to +4 positions (stem cells) and in +4 to +10 positions (TA cells). We defined the duration of the S phase in the human colonic epithelium as 6 hours based on the in vitro live imaging results using Fucci reporter organoids (not shown). We assumed that all cells were labeled with EdU when L_i (cell cycle length) < x (pulse duration) + 6 (length of S phase), and that the proportion of labeled cells was (x + 6)/L_i when L_i > x + 6. We set up an equation using the proportion of labeled cells at x = 24 and 96 (hr) and obtained the following solutions: L₁ (stem cell) = 7.1 days for x = 96 (hr), and L₁ (stem cell) = 7.3 days and L₂ (TA cell) = 1.5 days for x = 24 (hr).

Statistical Analysis

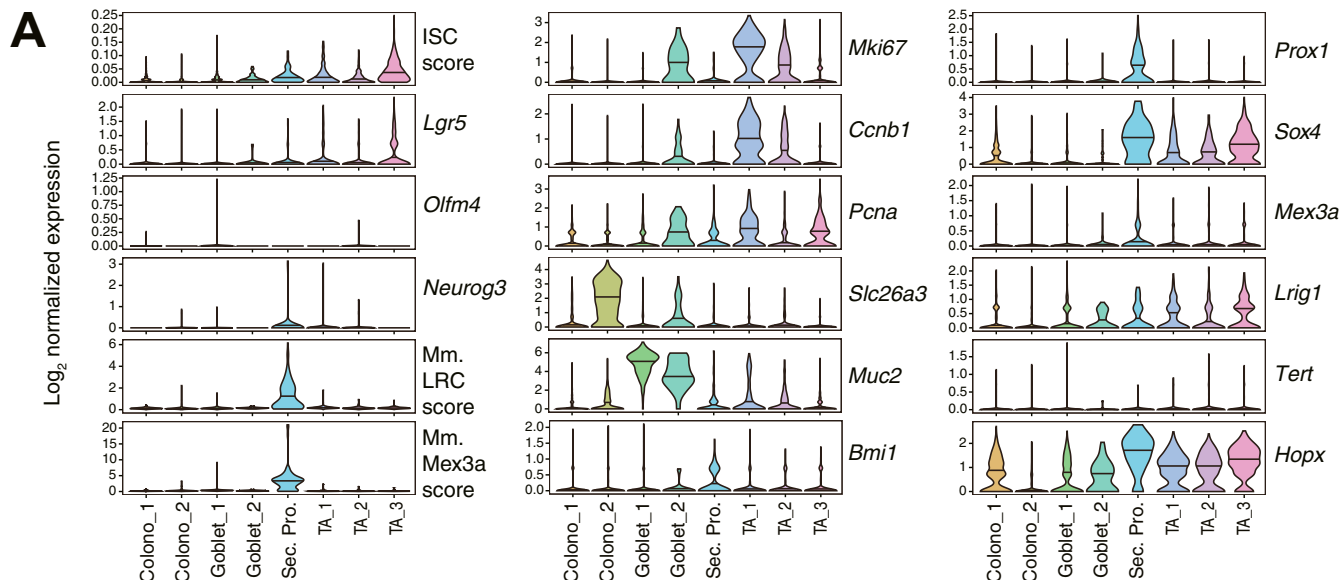
The comparison between separate groups was performed using unpaired 2-tailed *t*-test. The difference of clone sizes in control and 5-FU-treated groups in split-Cre experiments was analyzed using a linear mixed models and likelihood ratio test. The *P* value < .05 was defined as significantly different. Asterisks in the figures indicate the following *P* values: **P* < .05, ***P* < .01; ****P* < .001; n.s. *P* > .05. Statistical analysis and graph visualization was performed on the R software. The box in box-whisker plots demonstrates the interquartile range (Q1, Q3), with the median (Q2) as a line in the box. The upper whisker = Q3 + 1.5 (Q - Q1) and the lower whisker = Q1 - 1.5 (Q3 - Q1). Where given, N (the number of replicates) refers to the number of different individuals and mice.

Supplementary References

1. Fujii M, Shimokawa M, Date S, et al. A colorectal tumor organoid library demonstrates progressive loss of niche factor requirements during tumorigenesis. *Cell Stem Cell* 2016;18:827–838.
2. Sugimoto S, Ohta Y, Fujii M, et al. Reconstruction of the human colon epithelium in vivo. *Cell Stem Cell* 2018; 22:171–176.e5.
3. Ito M, Hiramatsu H, Kobayashi K, et al. NOD/SCID/gamma(c)null mouse: an excellent recipient mouse model for engraftment of human cells. *Blood* 2002; 100:3175–3182.
4. Fujii M, Matano M, Toshimitsu K, et al. Human intestinal organoids maintain self-renewal capacity and cellular diversity in niche-inspired culture condition. *Cell Stem Cell* 2018;23:787–793.e6.
5. Mihara E, Hirai H, Yamamoto H, et al. Active and water-soluble form of lipidated Wnt protein is maintained by a serum glycoprotein afamin/alpha-albumin. *Elife* 2016;5.
6. Shimokawa M, Ohta Y, Nishikori S, et al. Visualization and targeting of LGR5+ human colon cancer stem cells. *Nature* 2017;545:187–192.
7. Jullien N, Sampieri F, Enjalbert A, et al. Regulation of Cre recombinase by ligand-induced complementation of inactive fragments. *Nucleic Acids Res* 2003;31:e131.
8. Buczacki SJ, Zecchini HI, Nicholson AM, et al. Intestinal label-retaining cells are secretory precursors expressing Lgr5. *Nature* 2013;495:65–69.
9. Fujii M, Matano M, Nanki K, et al. Efficient genetic engineering of human intestinal organoids using electroporation. *Nat Protoc* 2015;10:1474–1485.
10. Guo Q, Mintier G, Ma-Edmonds M, et al. Cold shock increases the frequency of homology directed repair gene editing in induced pluripotent stem cells. *Sci Rep* 2018;8:2080.
11. Butler A, Hoffman P, Smibert P, et al. Integrating single-cell transcriptomic data across different conditions, technologies, and species. *Nat Biotechnol* 2018; 36:411–420.
12. Hafemeister C, Satija R. Normalization and variance stabilization of single-cell RNA-seq data using regularized negative binomial regression. *Genome Biol* 2019; 20:296.
13. Ahlmann-Eltze C, Huber W. glmGamPoi: fitting Gamma-Poisson generalized linear models on single cell count data. *Bioinformatics* 2021;36:5701–5702.
14. Tirosh I, Izar B, Prakadan SM, et al. Dissecting the multicellular ecosystem of metastatic melanoma by single-cell RNA-seq. *Science* 2016;352:189–196.
15. Barriga FM, Montagni E, Mana M, et al. Mex3a marks a slowly dividing subpopulation of Lgr5+ intestinal stem cells. *Cell Stem Cell* 2017;20:801–816.e7.
16. Parikh K, Antanaviciute A, Fawkner-Corbett D, et al. Colonic epithelial cell diversity in health and inflammatory bowel disease. *Nature* 2019;567:49–55.
17. Smillie CS, Biton M, Ordovas-Montanes J, et al. Intra- and inter-cellular rewiring of the human colon during ulcerative colitis. *Cell* 2019;178:714–730.e22.
18. Stuart T, Butler A, Hoffman P, et al. Comprehensive integration of single-cell data. *Cell* 2019;177:1888–1902.e21.
19. Brugger MD, Valenta T, Fazilaty H, et al. Distinct populations of crypt-associated fibroblasts act as signaling hubs to control colon homeostasis. *PLoS Biol* 2020;18:e3001032.
20. Herring CA, Banerjee A, McKinley ET, et al. Unsupervised trajectory analysis of single-cell RNA-seq and imaging data reveals alternative tuft cell origins in the gut. *Cell Systems* 2018;6:37–51.e9.
21. Potten CS, Al-Barwari SE, Hume WJ, et al. Circadian rhythms of presumptive stem cells in three different epithelia of the mouse. *Cell Tissue Kinet* 1977; 10:557–568.
22. Higasa K, Miyake N, Yoshimura J, et al. Human genetic variation database, a reference database of genetic variations in the Japanese population. *J Hum Genet* 2016;61:547–553.



Supplementary Figure 1. Single-cell characterization of the human colonic epithelium, related to **Figure 1**. (A) Gene expression patterns of human colonic epithelial cells based on cell clusters. Top 5 genes in each cluster are shown. (B) The expression of putative markers for mouse +4 cells and reserve stem cells in each cluster. (C) Integration of our and public human colon scRNA-seq datasets. The data were assembled into an integrated reference and shown as *uniform manifold approximation and projection (UMAP)* plots (top). Types (top left), cell cycle phase (top middle), and source study (right top) of each cell. Note that stem cells (red) are mainly in the G₁ phase. Cell types in each study are also shown (bottom). EEC, enteroendocrine cell; ILC, innate lymphoid cell.

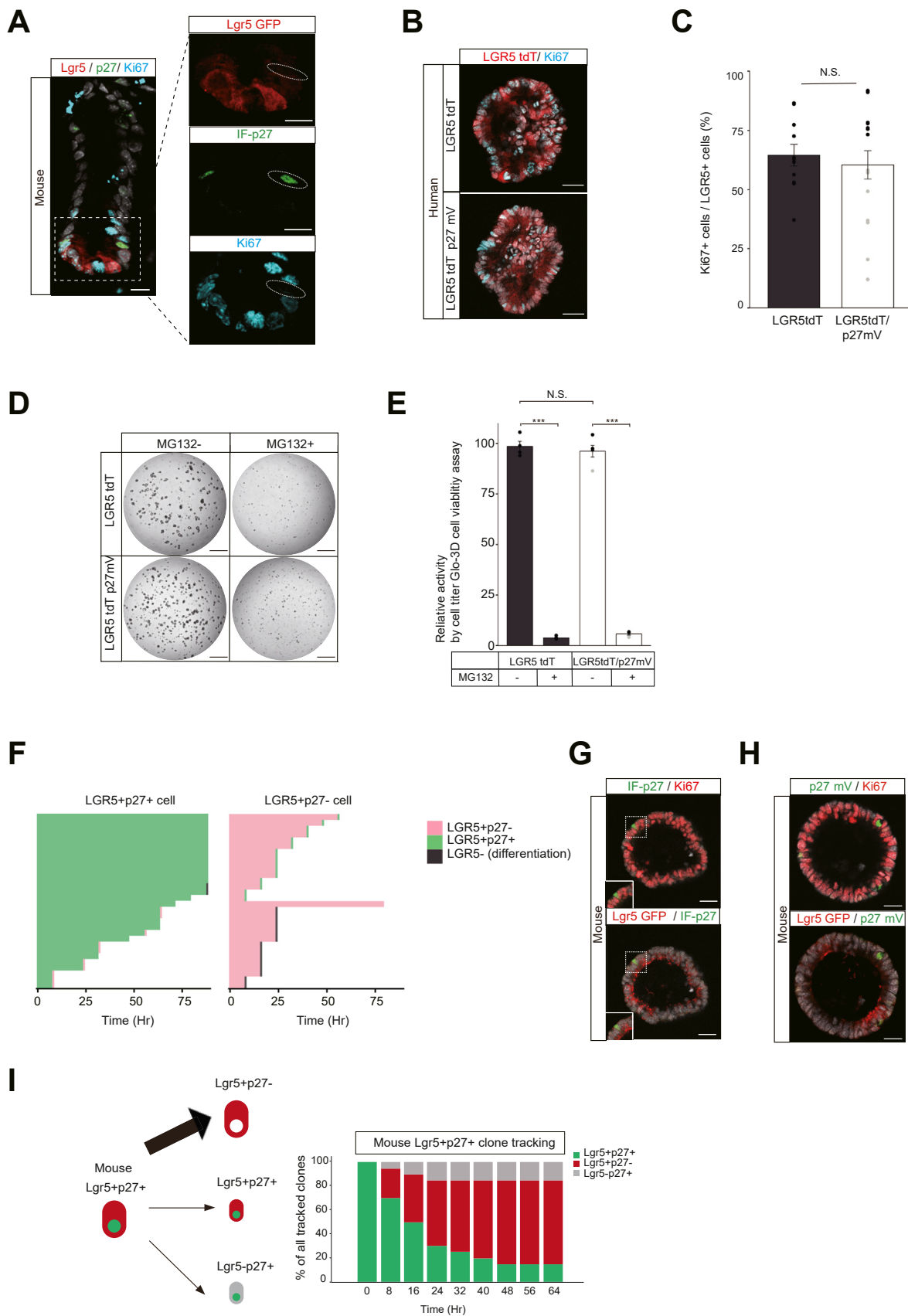


B

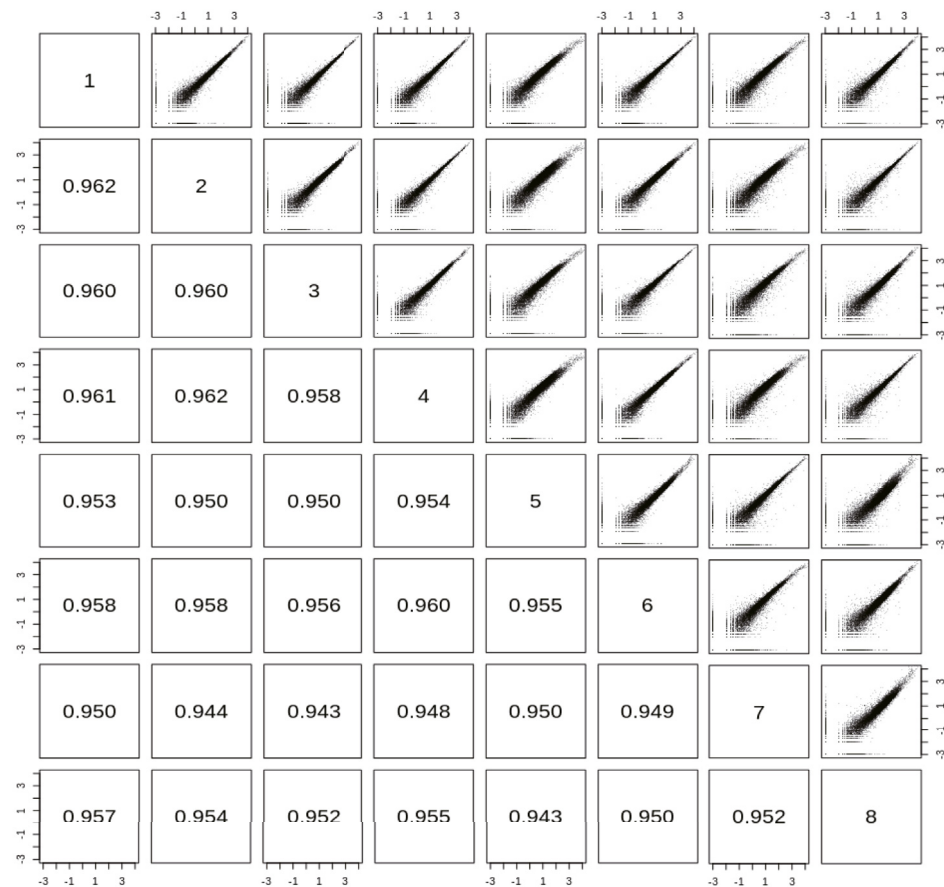
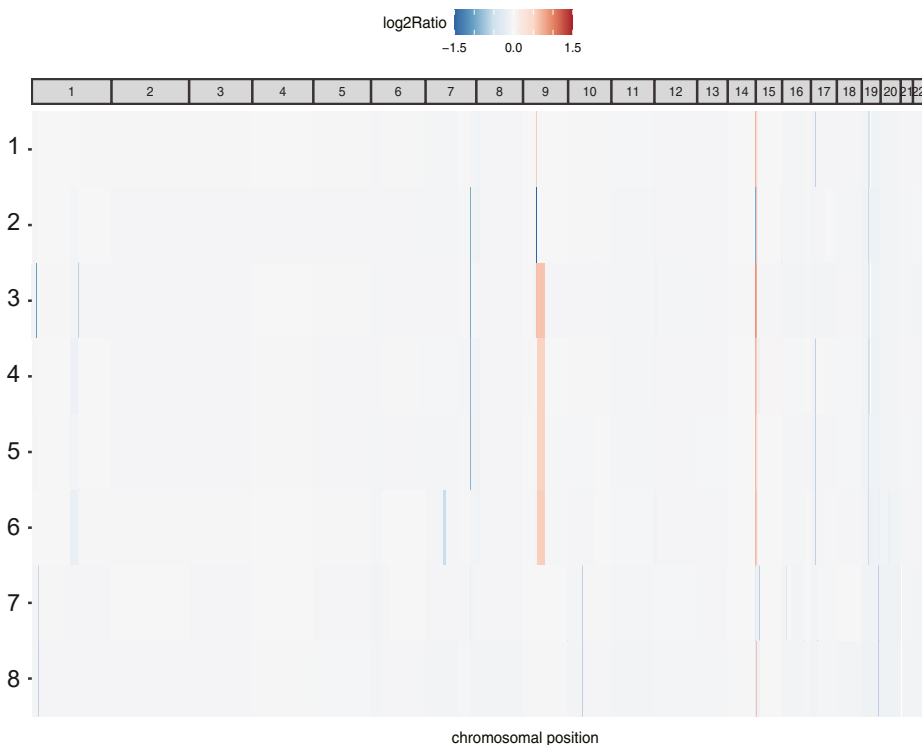
human+mouse classification										
	BEST4/ OTOP2	Colonocyte _1	Colonocyte _2	Goblet	Immature goblet	Secretory progenitor	TA_1	TA_2	TA_3	
Human classification	BEST4/OTOP2	400	11	20	3	0	4	13	9	9
	Colonocyte_1	0	905	301	0	0	0	0	146	6
	Colonocyte_2	0	6	668	0	2	0	0	0	0
	Goblet	0	0	0	1247	99	0	0	0	0
	Immature goblet	0	0	1	87	197	0	0	0	0
	Secretory progenitor	1	2	0	24	13	180	8	5	2
	TA_1	0	0	0	0	1	0	722	6	12
	TA_2	0	2	0	1	0	0	4	716	21
	TA_3	1	35	0	1	0	1	15	46	1042
Stem	0	1	0	0	0	0	0	0	107	

human+mouse classification									
	BEST4/ OTOP2	Colonocyte _1	Colonocyte _2	Goblet	Immature goblet	Secretory progenitor	TA_1	TA_2	TA_3
Human	402	962	990	1363	312	185	762	928	1199
Mouse	2	960	1526	1656	55	137	437	351	638

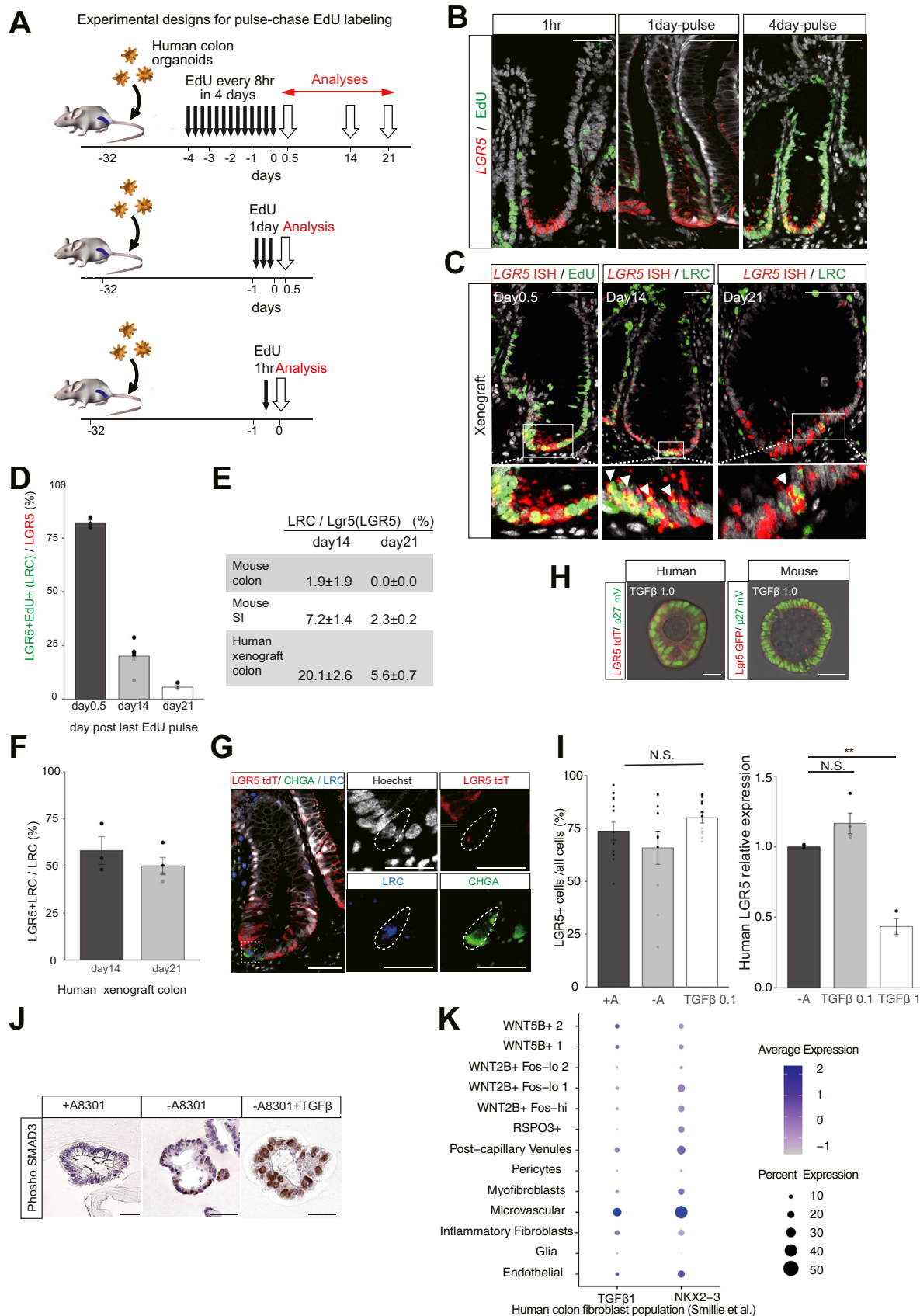
Supplementary Figure 2. Single-cell characterization of the human and mouse colonic epithelium, related to [Figure 1](#). (A) Expression of the indicated genes and gene sets in each cluster of the mouse colonic epithelial cells. The clusters were generated by the integration of human and mouse datasets as in [Figure 1C](#), and only mouse cells are shown here. The following genes and scores are shown; ISC genes (ISC score, *Lgr5* and *Olfm4*), secretory progenitor gene (*Neurog3*), LRC signature score, Mex3a signature score, cell cycle genes (*Mki67*, *Ccnb1*, and *Pcna*), differentiation-related genes (*Slc26a3* and *Muc2*), and markers for +4 /reserve stem cells in the mouse small intestine (*Prox1*, *Sox4*, *Mex3a*, *Lrig1*, *Tert*, and *Hopx*). The levels of ISC, LRC, and Mex3a signature scores refer to the percentage of signature gene transcripts. The expression of single genes is shown in log₂-transformed normalized counts. (B) Comparison of clustering results of human only and human+mouse-combined cellular classification.



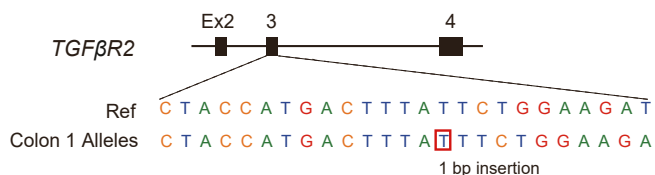
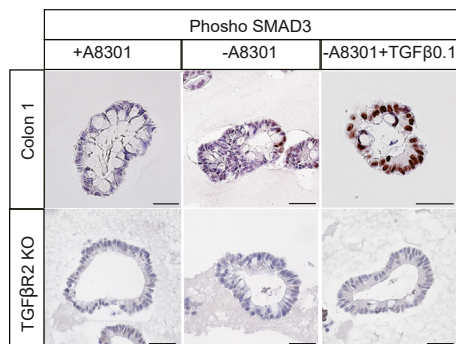
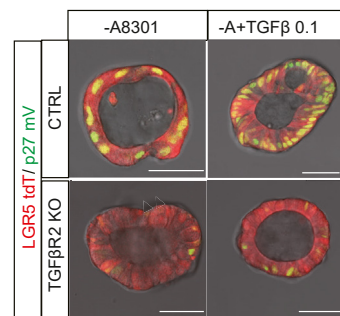
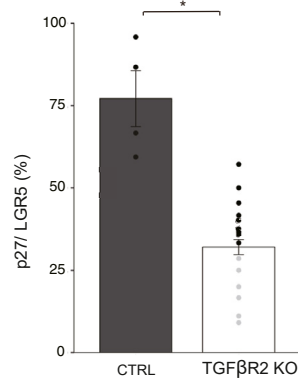
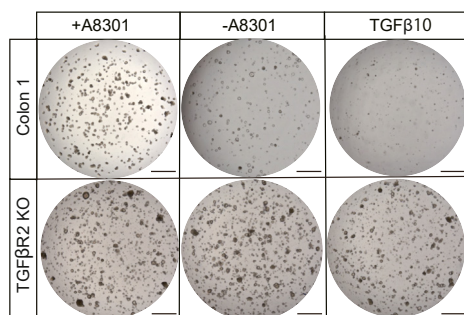
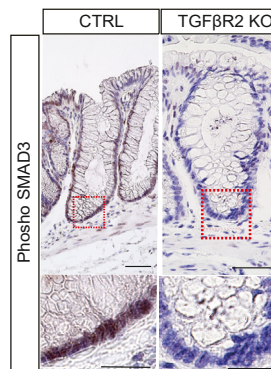
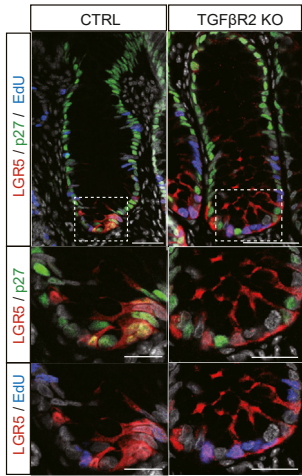
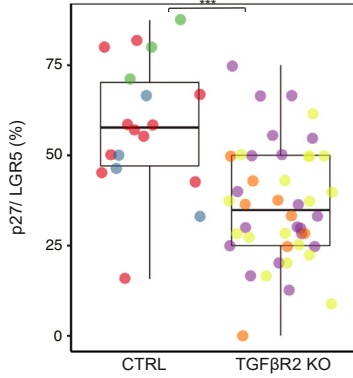
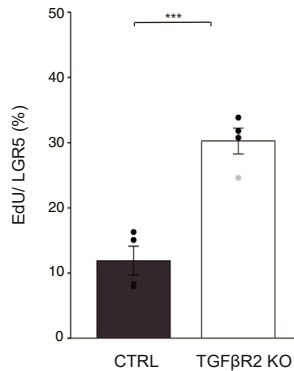
←
Supplementary Figure 3. Validation and labeling of p27 in human and mouse LGR5 (Lgr5) stem cells, related to [Figure 2](#). (A) Co-staining of p27 (green), Ki67 (cyan), and Lgr5-GFP reporter (red) in the mouse colon. White circle outlines an Lgr5^{low} p27⁺ Ki67⁻ cell. Scale bar: 10 μ m. (B) Representative images of Ki67 staining in human LGR5-tdTomato (tdT) (top) and LGR5-tdTomato/p27-mVenus (mV) (bottom) organoids. Scale bar: 25 μ m. (C) The percentage of Ki67⁺ cells in LGR5⁺ cells in human LGR5-tdTomato and LGR5-tdTomato/p27-mVenus organoids. NS, not significant (Welch's unpaired *t* test). Data are shown as mean \pm SEM. Each dot represents 1 organoid. n = 11 organoids for LGR5-tdTomato and 16 organoids for LGR5-tdTomato/p27-mVenus. (D) Representative images of LGR5-tdTomato (tdT) and LGR5-tdTomato/p27-mVenus (mV) organoids cultured from 1000 single cells. Scale bar: 1 mm. (E) The viability of LGR5-tdTomato and LGR5-tdTomato/p27-mVenus organoids measured with ATP luminescence (MG132, 0.125 μ M). Conditions shown in (D) were used. Welch's unpaired *t* test. (F) Tracking of the cell fate of LGR5⁺p27⁺ (left) and LGR5⁺p27⁻ (right) clones by *in vitro* live imaging. Each row corresponds to 1 clone. The black bar indicates a loss of LGR5⁺ cells in the clone. The pink bar indicates a conversion from LGR5⁺p27⁺ to LGR5⁺p27⁻ cells. The green bar indicates the emergence of at least one LGR5⁺p27⁻ cell in the clone. (G) Representative immunofluorescence (IF) images of p27 (green) and Ki67 (red, top) staining in mouse colonic organoids. Lgr5-GFP fluorescence was superimposed (red, bottom). Insets show a rare Lgr5⁺ Ki67⁻ p27⁺ cell. Scale bar: 25 μ m. (H) Representative images of p27-mVenus (green) and Ki67 (red, top) staining, and Lgr5-GFP (red, bottom) expression in mouse colonic organoids. Scale bar: 25 μ m. (I) Fate tracking of mouse Lgr5⁺ p27⁺ cells by live imaging of Lgr5-GFP(DTR)/p27-mVenus mouse colonic organoids. A schematic diagram of the possible cell fates (left). The percentage of each cell fate in all tracked Lgr5⁺ p27⁺ clones at multiple time points is shown on the right. No Lgr5⁺ p27⁺ clones became Lgr5⁻ p27⁻ during the observation period. n = 28 clones from 7 mouse organoids were analyzed. Nuclear counterstaining: Hoechst33342 (A, B, G, and H). Inset shows higher magnification (A, G).

A**B**

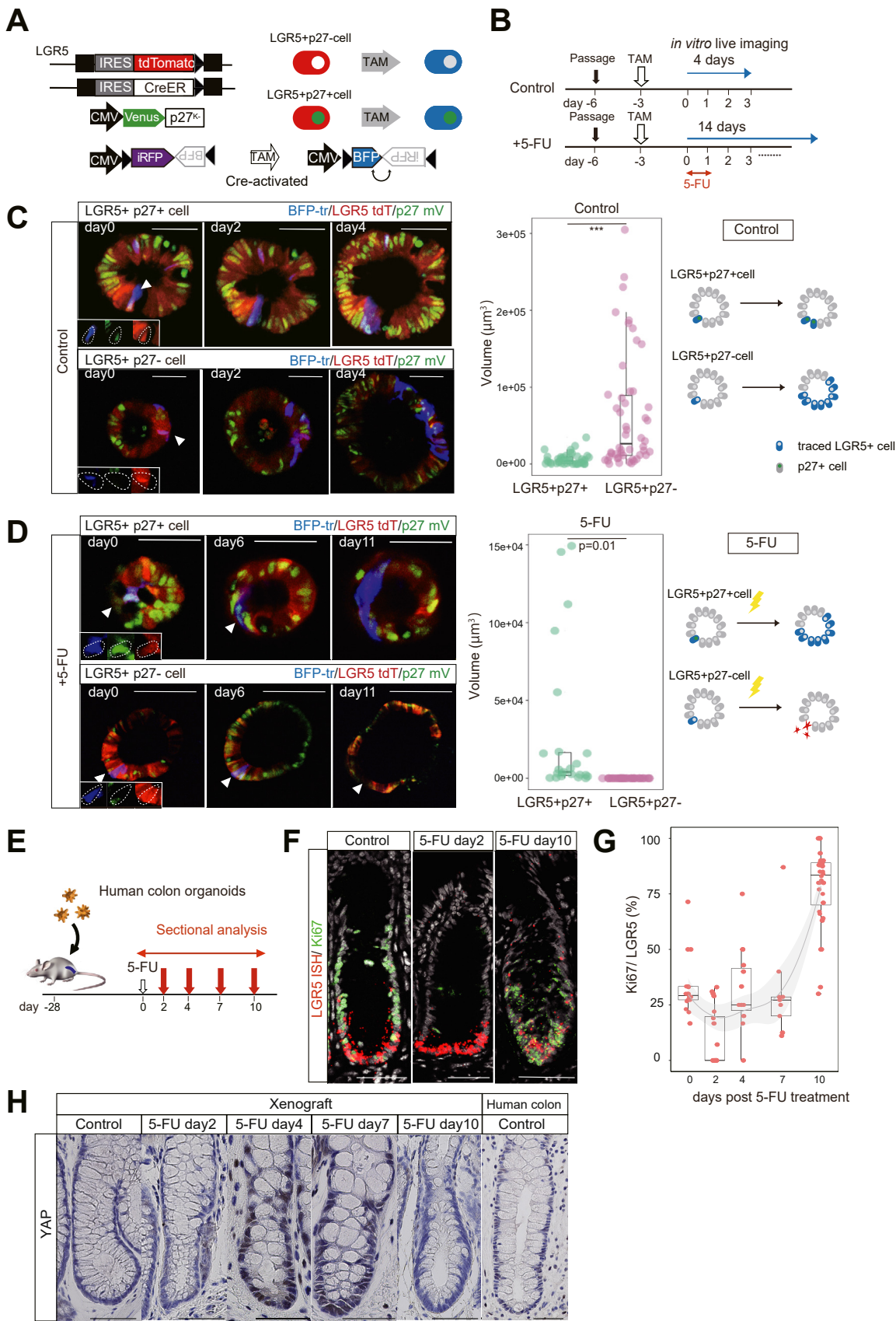
Supplementary Figure 4. Global expression and genotype of nonengineered, gene-engineered, and post-xenotransplanted human organoids, related to [Figure 3](#). (A) Pearson's correlation of the transcriptomes of nonengineered, gene-engineered, and post-xenotransplanted organoids. $\log_{10}(\text{transcripts per million} + 0.001)$ values of all genes were used for comparison. The identity of each organoid is as follows; 1: patient 1 nonengineered organoids, 2: patient 1 LGR5-iCT organoids (single knock-in), 3: patient 1 LGR5-tdTomato/p27 split-Cre organoids (double KI), 4: patient 1 post-xenotransplanted LGR5-iCT GFP organoids from mouse #1, 5: patient 1 post-xenotransplanted LGR5-iCT GFP organoids from mouse #2, 6: patient1 post-xenotransplanted LGR5-iCT GFP organoids from mouse #3, 7: patient 2 nonengineered organoids, and 8: patient 2 LGR5-iCT organoids. (B) Exome-based DNA copy-number analysis. The chromosome region in 9p had few single nucleotide polymorphisms in our panel of normal used in the analysis, and the gain-like regions in organoids 3–7 are considered to be artefacts based on in-depth interrogation of the regional allele frequency. Organoid IDs refer to those in (A).



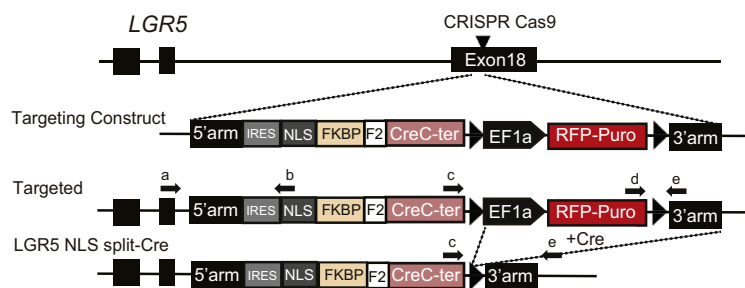
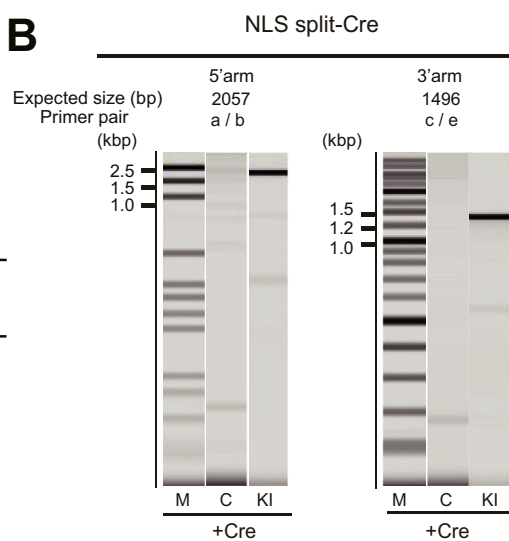
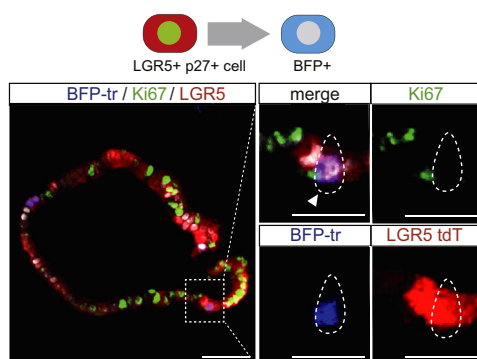
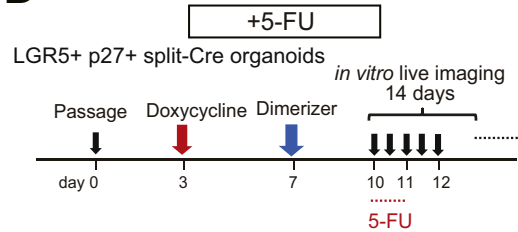
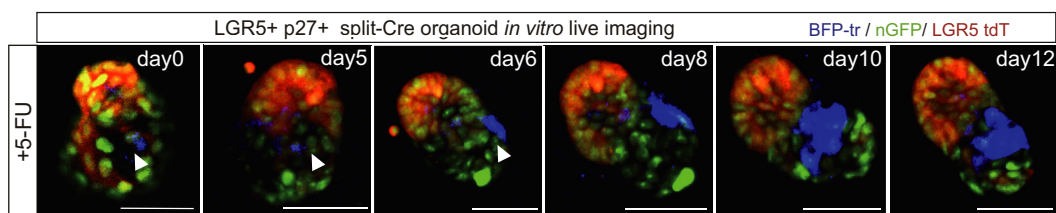
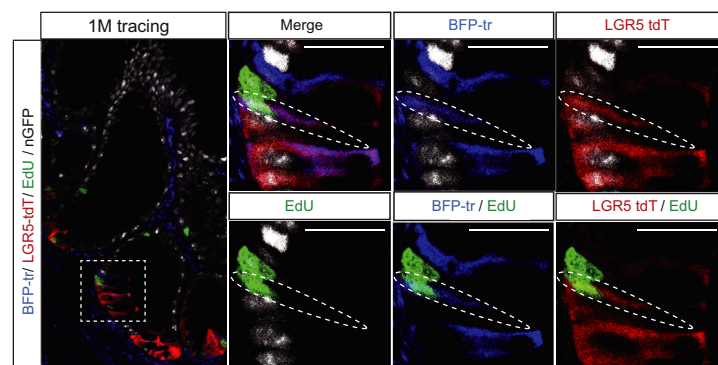
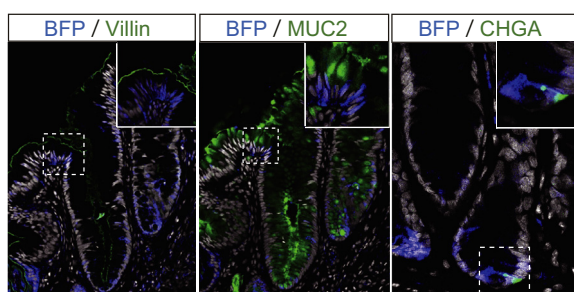
Supplementary Figure 5. LRCs in orthotopic xenografts, related to Figure 3. (A) Experimental designs for pulse-chase EdU labeling in orthotopically xenotransplanted human colon organoids. (B) Representative images of EdU labeling (green) and LGR5-ISH/LGR5-tdTomato (red) immediately after EdU treatment with the indicated pulse durations. Scale bar: 50 μ m. (C) Representative images of LGR5 ISH (red) and EdU signal (green) on day 0.5, 14, and 21 after a 4-day EdU administration. EdU⁺ cells on day 14 (middle) and day 21 (right) were defined as LRCs. Scale bar: 50 μ m. (D) The proportion of LRCs (EdU⁺ cells) in all LGR5⁺ cells at the indicated time points after a 4-day EdU treatment. Each dot represents 1 mouse. n = 25 crypts from 3 mice (day 0.5), n = 53 crypts from 6 mice (day 14), and n = 35 crypts from 4 mice (day 21) were analyzed. (E) The percentage of LRCs in all Lgr5 (LGR5)⁺ cells in the mouse colon, small intestine (SI) and human xenograft colon on day 14 and day 21 after a 4-day treatment with EdU. n = 11 (day 14, colon), 81 (day 21, colon), 92 (day 14, SI), and 79 crypts (day 21, SI) from 3 mice were analyzed. The data on human xenograft colon derive from the measurement in Supplementary Figure 5D. (F) The percentage of LGR5⁺ cells in all LRCs in orthotopic human colon xenografts on day 14 and day 21 after a 4-day treatment with EdU. n = 24 crypts from 4 mice (day 14) and n = 38 crypts from 3 mice (day 21). (G) Representative images of Chromogranin A staining (CHGA, green), LGR5 tdTomato expression (red), and EdU retention (LRC, blue) in a orthotopic xenograft. Scale bar: 50 μ m (left), 25 μ m (right). (H) Representative images of LGR5-tdTomato and p27-mVenus fluorescence in human colonic organoids (left) and Lgr5-GFP(DTR) and p27-mVenus expression in mouse colonic organoids (right) treated with recombinant TGF- β 1 (1 ng/mL for 24 hours) in an A83-01-free condition. Scale bar: 10 μ m. (I) The percentage of LGR5⁺ cells in all organoid cells cultured with the indicated conditions (left). Data are shown as mean \pm SEM. Each dot represents 1 organoid. NS, not significant (Welch's t test). n = 13, n = 9, and n = 11 organoids were analyzed for A83-01-added, A83-01-removed and TGF- β 1-added (0.1 ng/mL for 24 hours) conditions, respectively. Quantitative polymerase chain reaction analysis for LGR5 in all organoids cells cultured with the indicated conditions (right). n = 3, n = 3, and n = 4 organoids were analyzed for A83-01-removed and TGF- β 1-added (0.1 ng/mL and 1 ng/mL for 24 hours). Data are shown as mean \pm SEM. NS for A83-01-removed and TGF- β 1-added (0.1 ng/mL) condition. **P < .01 for A83-01-removed and TGF- β 1-added (1 ng/mL) condition (1-way analysis of variance, followed by Tukey's post-hoc test). (J) Representative images of phospho-SMAD3 staining in organoids cultured with the indicated conditions. Scale bar: 25 μ m. (K) Average expression of TGF- β 1 and NKX2-3 and percentage of cells expressing them in each cell cluster on human fibroblast population using the public scRNA-seq datasets. Nuclear counterstaining: Hoechst 33342 (B, C, and G). Inset shows higher magnification (C, G).

A**B****D****E****C****F****G****H****I**

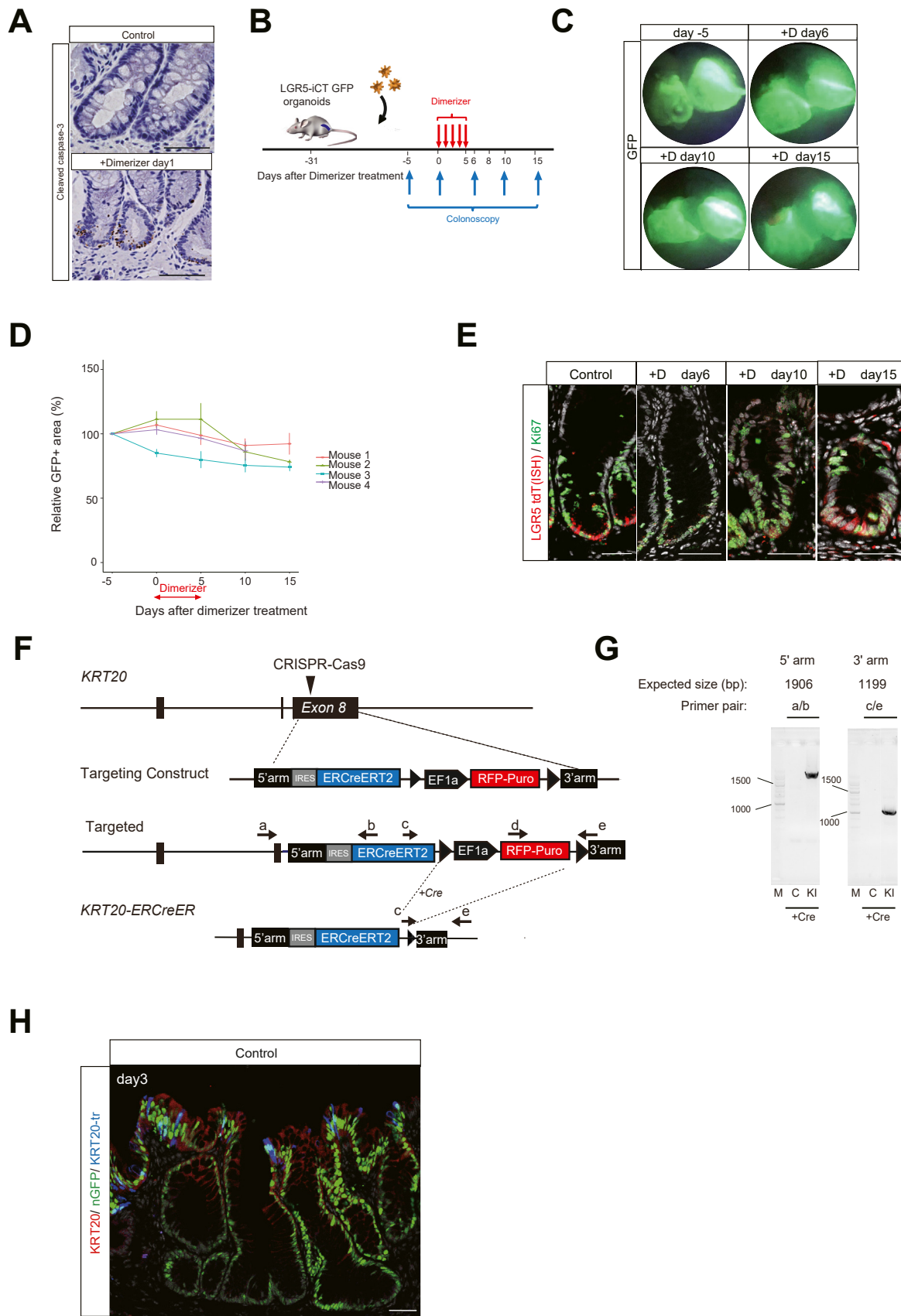
Supplementary Figure 6. TGF- β R2 knocked-out organoids reduce the proportion of p27 to LGR5⁺ cells, related to [Figure 3](#). (A) Construction of TGF- β R2 knocked-out organoids. (B) Representative images of phospho-SMAD3 staining in control (*top*) and TGF- β R2-KO organoids (*bottom*) cultured with the indicated conditions. Scale bar: 25 μ m. (C) Representative images depicting resistance to the absence of A83-01 and addition of TGF- β 1 (10 ng/mL) in TGF- β R2-KO organoids. Scale bar: 1 mm. (D) LGR5-tdTomato and p27-mVenus fluorescence in the absence of A83-01, or with TGF- β 1 (0.1 ng/mL) in an A83-01-free condition for control and TGF- β R2-KO organoids. Scale bar: 50 μ m. (E) The percentage of p27⁺ cells to LGR5⁺ cells for control and TGF- β R2-KO organoids cultured in an A83-01-free condition. A dot represents each organoid. $P = .01$ (Welch's *t* test). (F) Phospho-SMAD3 staining in control and TGF- β R2-KO orthotopic xenograft. Scale bar: 50 μ m (*top*), 20 μ m (*bottom*). The images in control xenograft are used in [Figure 3H](#). (G) LGR5-tdTomato, p27-mVenus fluorescence and 1hr-EdU staining in control and TGF- β R2-KO xenograft. Scale bar: 50 μ m (*top*), 20 μ m (*bottom*). (H) The percentage of p27⁺ cells in LGR5⁺ cells for control and TGF- β R2-KO xenograft. *** $P < .001$ ($n = 22$ crypts for control, $n = 44$ crypts for TGF- β R2-KO). (I) The percentage of EdU⁺ cells in LGR5⁺ cells for control and TGF- β R2-KO xenograft. *** $P < .001$ ($n = 31$ crypts for control, $n = 53$ crypts for TGF- β R2-KO).



Supplementary Figure 7. LGR5⁺p27⁺ cells withstand and are activated upon 5-FU-induced injury, related to [Figure 4](#). (A) Generation of LGR5-tdTomato/LGR5-CreER/p27-mVenus organoids that enable visualization of LGR5 and p27, and LGR5 lineage tracing. Tam, tamoxifen. (B) Schedule for in vitro live imaging of LGR5 lineage tracing in LGR5-tdTomato/LGR5-CreER/p27-mVenus organoids. (C) Representative images from in vitro live imaging of LGR5 lineage tracing from a single LGR5⁺p27⁺ cell (top) and LGR5⁺p27⁻ cell (bottom) without 5-FU treatment (left). White arrowhead and dotted outline in insets show examples of traced LGR5⁺p27⁺ and LGR5⁺p27⁻ cells. Scale bar: 50 μ m. The size of clones traced from LGR5⁺p27⁺ cells and LGR5⁺p27⁻ cells on day 4 after tracing (middle). Each dot represents a tracked clone. ***P < .001, Welch's t test. n = 42 and n = 50 clones were tracked from LGR5⁺p27⁺- and LGR5⁺p27⁻ cells, respectively. A schematic diagram of the cell fate of LGR5⁺p27⁺ and LGR5⁺p27⁻-derived clones without 5-FU treatment (right). (D) Representative images from in vitro live imaging of LGR5 lineage tracing from a single LGR5⁺p27⁺ cell (top) and LGR5⁺p27⁻ cell (bottom) after 5-FU treatment. White arrowhead and dotted outline in insets show examples of traced LGR5⁺p27⁺ and LGR5⁺p27⁻ cells. White arrowhead in top images indicates an LGR5⁺p27⁺ clone that expanded after a 5-FU treatment. White arrowhead in bottom images indicates an LGR5⁺p27⁻ clone, which newly expressed p27 by day 2 and diminished by day 7 post 5-FU treatment. Scale bar: 50 μ m. The size of clones traced from LGR5⁺p27⁺ cells and LGR5⁺p27⁻ cells on day 14 post-5-FU treatment (middle). Each dot represents a tracked clone. P = .01, Welch's t test. n = 23 and n = 38 clones were tracked from LGR5⁺p27⁺- and LGR5⁺p27⁻ clones, respectively. The schematic diagram of the cell fates of LGR5⁺p27⁺ and LGR5⁺p27⁻-derived clones after 5-FU treatment (right). (E) Schedule for the analysis of xenograft sections after 5-FU treatment. (F) Representative images of Ki67 co-staining (green) with LGR5 ISH (red) in engrafted human colon crypts on day 0, 2, and 10 post 5-FU treatment. Scale bar: 50 μ m. Nuclear counterstaining, Hoechst 33342. (G) The percentage of Ki67⁺ cells in all LGR5⁺ cells on day 0, 2, 4, 7, and 10 post 5-FU treatment. A dot represents each crypt. The gray line shows the data smoothed using local polynomial regression, and the light gray area shows the 95% CI. n = 20 (day 0), 21 (day 2), 15 (day 4), 9 (day 7), and 32 (day 10) crypts. (H) Representative images of YAP staining in the xenografted human colons at multiple time points post 5-FU treatment (left), and YAP staining in human colon (right). Scale bar: 50 μ m. LGR5⁺ cell-derived BFP⁺ clone, blue; LGR5-tdTomato, red; p27-mVenus, green (C, D). White arrowhead indicates single clones used for tracking (C, D). Boxes demarcate first and third quartiles; bars represent median values; whiskers represent the distances of 1.5 times inter-quartile ranges (C, D, and G).

A**B****C****D****E****F**

Supplementary Figure 8. Validation of LGR5⁺p27⁺ split-Cre organoids, related to Figure 5. (A) Targeting strategy for the knock-in of CreC downstream of LGR5. The locations of polymerase chain reaction primers, the CRISPR target site, and *loxP* sites are indicated. Primer pairs a/b and c/e detect knock-in of the 5' and 3' arms of nuclear localization sequence split-Cre, respectively. (B) Validation of knock-in by genomic polymerase chain reaction using the primers shown in (A). C, control organoids; KI, knock-in organoids; M, size marker. (C) Validation of the split-Cre system. Fluorescence images of LGR5⁺p27⁺ tracing (BFP, blue), Ki67 staining (green), nuclear GFP (white), and LGR5-tdTomato (red) are shown for a single traced cell. White arrowhead and white-dotted line indicate the BFP⁺ cell. Scale bar: 50 μ m (top left), and 30 μ m (others). (D) Schedule for the in vitro live imaging of LGR5⁺p27⁺ split-Cre knock-in organoids after 5-FU treatment. (E) Representative images from in vitro live imaging of LGR5⁺p27⁺ split-Cre knock-in organoids after 5-FU treatment. White arrowhead indicates a BFP-traced cell. BFP-traced cell (blue); nuclear GFP (green); LGR5-tdTomato (red). Scale bar: 50 μ m. (F) Differentiated cells in lineage-traced BFP⁺ crypts of control mice at day 90. Villin, MUC2, and CHGA staining depict enterocytes, goblet cells, and enteroendocrine cells, respectively. Scale bar: 50 μ m. (G) EdU staining and traced-BFP⁺ clones in control xenografts at day 28. EdU was administered 1 hour before sacrifice. Dotted outline shows an EdU⁺BFP⁺LGR5⁺ cell. Scale bar: 50 μ m (left), 20 μ m (others).



Supplementary Figure 9. Validation of LGR5⁺ cell ablation and KRT20⁺-ERCreER lineage tracing, related to [Figure 6](#). (A) Representative images of cleaved caspase-3 staining after dimerizer treatment. Scale bar: 50 μ m. (B) Schedule for colonoscopic observation of orthotopic xenografts after LGR5 ablation. (C) Representative images of GFP⁺ xenograft areas by colonoscopic observation at multiple time points shown in [Supplementary Figure 9B](#). (D) Relative GFP⁺ xenograft area at multiple time points after dimerizer treatment. Each xenograft area in a mouse was measured at multiple time points using a biopsy forceps as a size reference. Each mouse is shown by a different color. (E) Representative images of Ki67 co-staining with LGR5-tdTomato (or LGR5 *in situ* hybridization [ISH]) after dimerizer treatment at multiple time points. Scale bar: 50 μ m. (F) Targeting strategy for the generation of human KRT20⁺-ERCreER knock-in organoids. (G) Gel electrophoresis of polymerase chain reaction products from knocked-in organoids using the primers shown in (F) and [Supplementary Table 1](#). C, control organoids, KI, knock-in organoids; M, size marker. (H) Representative image of KRT20 staining in a KRT20⁺-ERCreER nGFP-BFP reporter xenograft on day 3 post tamoxifen (Tam) treatment. KRT20 staining (red), nGFP (green), and KRT20-traced cell (BFP). Scale bar: 50 μ m.

Supplementary Table 1. Polymerase Chain Reaction Primers, Probes, CRISPR Target Sites, and Homology Arms Used in This Study, Related to [Supplementary Methods](#)

Variable	PCR primers	Sequence (5' to 3')
LGR5-KI	LGR5 F (a) iCasp9 R (b) tdTomato R (b) loxP F (c) tdTomato F (c) puro F (d) LGR5 R (e) CreERT2 R (b) FKBP R (b) CreERT2 F(c) CreC F(c)	TGGCATCTAAATAAGAGACAAAAGGGTA CTCGGATCACCTCCTGCTGCCTA AGCGCATGAACTCTTGATGACCTC GATCTGATCTTCCACTCAAACATATAACT CTGTTCTGTACGGCATGGACGA CCCGCAACCTCCCCCTTACGAG ATCAAAGAATATGCCACTGTACAAGGTT TCTTGCACCTCATCACTCGTTGCAT CTCGGATCACCTCCTGCTGCCTA GGCACATGAGTAACAAAGAATGGAGCATC CTGGTGTGTCATCCCTGAAATCATGC
KRT20-KI	KRT20 F (a) EGFP R (b) CreERT2 R (b) loxPF(c) puro F (d) KRT20R (e)	AGGAGTGCATTCCATTTCAAAACAGC GATGAACCTCAGGGTCAGCTTGCCTGA TCTTGCACCTCATCACTCGTTGCAT GATCTGATCTTCCACTCAAACATATAACT CCCGCAACCTCCCCCTTACGAG AGCACACATTGATTTCCTCATAAACAA
CRISPR		Sequence (5' to 3') + PAM
LGR5-1 LGR5-2 LGR5-3 KRT20-1 KRT20-2		GTAATAATAAGAAGAGCTG AGG TGTCTTAATTAAATATGTGA AGG ATCTCTCAGTTAGTAAGAA AGG TTAAATATTCTAGTGCTCAC TGG ATTACAGAGTCTGATAAT AGG
Homology arms		Genomic location
LGR5 5' LGR5 3' KRT20 5' KRT20 3'		chr12: 71,583,717-71,584,731 chr12: 71,584,874-871,585,979 chr17: 40,876, 361-40, 877,414 chr17:40,875, 089-40, 876, 088

PAM, protospacer adjacent motif; PCR, polymerase chain reaction.